Title
Structural Characterization of Filled n-type IrSb3 Skutterudites

Author
Nguyen, Diep Thi Ngoc

Publication Date
2014

Peer reviewed|Thesis/dissertation

UNIVERSITY OF CALIFORNIA

Los Angeles

Structural Characterizations of Filled n-type $IrSb_3$ Skutterudites

A thesis submitted in partial satisfaction of the Requirements for the degree Master of Science in Chemistry

by

Diep Thi Ngoc Nguyen

2014

ABSTRACT OF THE THESIS

Structural Characterizations of Filled n-type $IrSb_3$ Skutterudites

By

Diep Thi Ngoc Nguyen

Master of Science in Chemistry

University of California, Los Angeles, 2014

Professor Richard B. Kaner, Chair

Thermoelectric (TE) materials have been attractive to research groups all over the world for their ability to directly convert thermal energy into electrical energy by the Seebeck effect, and vice versa by the Peltier effect. Due to their reliability and scalability, TE materials can be incorporated into devices for power generation or for cooling applications. Skutterudites have a complex crystalline structure in which the voids in the structure can be filled with foreign atoms. This doping technique has been shown to improve the TE performance of these "filled" skutterudite materials by disrupting the thermal conductivity without significantly impacting the electrical conductivity. Several studies have been done on filled $CoSb_3$-based skutterudites and high ZT values have been obtained for these materials around 600^{o}C. However, for thermoelectric applications that require higher operating temperatures, the more refractory $IrSb_3$

with a peritectic decomposition at 1136^0C (1409 K) offers an advantage over $CoSb_3$, which decomposes at 874^0C (1147 K). Using the traditional synthesis method of melting, quenching, then annealing stoichiometric amounts of the elements to produce n-filled skutterudites, the obtained filling fraction was found to be significantly lower than the nominal filling fraction due to the high reactivity, or sometimes the high volatility, of the elemental fillers. In this experiment, we explored the effects of pre-reacting the reactive metal filler element with one of the elements in the skutterudite structure and utilized this precursor for the synthesis of the filled skutterudites to compare the relative successes of achieving targeted filling percentages of the voids in the structure. $K_yIr_4Sb_{12}$ samples were synthesized using both the pure filler element, as well as the pre-reacted K-Sb compound. The phase purities, lattice parameters and elemental compositions were analyzed for each sample, calculated using X-ray diffraction (XRD), scanning electron microscopy (SEM) and electron microprobe analysis (EPMA), respectively. Their thermoelectric properties were also measured and calculated at room temperature and as a function of temperature ranging from room temperature to about 750^0C (1023 K). The preliminary results obtained suggest that pre-reacting the potassium with antimony results in higher percentages of phase impurities and less efficient void filling in $IrSb_3$ skutterudites. The highest ZT among all potassium-filled samples synthesized was measured to be 0.28 at 500^0C (773 K) for $K_{0.24}Ir_4Sb_{12}$. The data suggest that the cumulative thermoelectric properties of potassium filled $IrSb_3$ are not as favorable as those of $IrSb_3$-based skutterudites filled with other atoms such as Ba or Eu. However, some of the potassium-filled samples achieved high room temperature carrier concentrations, similar to those seen in barium-filled samples, indicating that the potassium effectively participates in doping the structure. This work has compared and contrasted two methods for incorporating potassium fillers in the void spaces of $IrSb_3$

skutterudites. While the ZT of potassium-filled samples was less than required for practical applications, this work does suggest that potassium may be useful in tuning electrical properties in samples that employ multiple element filling.

The relationship between the lattice parameter and the filling fraction was also studied on barium-filled and europium-filled $IrSb_3$ skutterudite samples. A higher nominal filling fraction achieved a higher EPMA filling fraction and a larger lattice parameter until the filling fraction limit was reached. While barium displayed higher filling efficiency, europium possessed a higher filling fraction limit. These preliminary results suggest that the optimization of multiple element filling to produce higher ZT is very obtainable with further studies on different single fillers.

The thesis of Diep Thi Ngoc Nguyen is approved.

Xiangfeng Duan

William M. Gelbart

Richard B. Kaner, Chair

University of California, Los Angeles

2014

This work is dedicated to my family, my teachers, my friends… my inspiration and my support.

Table of Contents

Acknowledgement

For the past twenty five years, I cannot express how grateful I am to my parents, who are always by my side, no matter what decision I make and no matter how far away I depart from home. Without them, I would not be who I am today and I would not be able to do what I have done and have been doing. Thank you, mom and dad, for your unconditional love and for always being there for me, whenever I need you.

I am also thankful to my younger sisters, who always know how to make me feel better when I struggle with various things at school and in life. Thank you for not insulting me when I fail and especially for not overly praising me when I succeed.

I am truly thankful for the support and continual encouragement that I have received from my advisor, Dr. Richard B. Kaner. I sincerely appreciate all the generous help and advice he has provided. Thank you for teaching my favorite courses at UCLA, Inorganic Chemistry and Solid State Chemistry, the ones that raised and strengthened my interests in my current field of work.

I would also like to send my special thanks to my mentor, Dr. Daniel J. King, Jr. for his constant support and guidance. I am so fortunate to have such a knowledgeable, caring, motivating, inspirational, and kindhearted mentor.

Very importantly, I must thank the entire Kaner Group for their genuine guidance and contribution. I have enjoyed the time I have spent with the Kanerites in the past 3 years, which is truly amazing and incredible.

I want to express my sincere gratitude to the Department of Chemistry and Biochemistry at UCLA for offering several useful classes for both of my undergraduate and graduate programs. I really appreciate the Departmental Scholars Program, which helps me to earn both a

Bachelor's degree in Chemistry and a Master's degree in Inorganic Chemistry in a shorter amount of time than other traditional master's programs.

I also want to send my special thanks to my departmental advisor, Melissa Woehrstein for her kind concerns at times when I fell behind my progress and for her very quick assistance whenever I needed help or had any questions.

Along my academic journey, there have been several significant teachers that have created great influence on my career path and to whom I want to show my great appreciation. Thank you Dr. Craig Merlic, Dr. Benjamin Schwartz, Dr. William Gelbart, Dr. Joseph Loo, Dr. Paula Diaconescu, Dr. Anastassia Alexandrova, Dr. Jeffrey Zink, Dr. Xingfeng Duan, Dr. Louis Bouchard, Dr. Heather Tienson, Dr. Steven Clarke, Dr. Chanfreau Guillaume, Dr. Yunfeng Lu, Dr. Carol Newton and Dr. Max Kopelevich for your helpful classes during my time at UCLA. I appreciate how interesting and challenging your classes were, which made the results much more rewarding.

Thank you Dr. Cinzia Muzzi, Dr. Brian McCauley, Dr. Beth McPartlan, Dr. Donald Francis, Dr. Mehrdad Khosravi, Dr. Stephanie Dickson and Dr. David Newton for your enthusiasm in teaching your knowledge and for helpful and fun classes at De Anza College.

Thank you Dr. Franklin Ow, Dr. Alan Khuu, Dr. Fang Tuan, Dr. Fernando Fernandez, Dr. Daniel Judge, Dr. Albert Lam for being my teachers and intensifying my love towards science at East Los Angeles College.

I am also really grateful to Mr. Tao Nguyen, Mr. Yen Nguyen, Mrs. Kim-Ngoc Nguyen, Mrs. Hoa Nguyen, Mr. Hiep Nguyen, Mr. Kien Nguyen, Mrs. Tu-Hau Hoang, Mr. Nam Nguyen, Dr. Hanh Van Nguyen, Dr. Yen-Nhi Nguyen, Mrs. Thao Pham, Mr. Trong Phan, Mrs. Ngoc Tran, Mrs. Xuan Nguyen, Mrs. Lan-Phuong Nguyen for having taught me not only academic

knowledge but also disciplines and important moral values during my teenager years. Without each of you, there must have been significant gaps not only in my knowledge but also in my conscience.

And last but not least, I want to thank my wonderful friends, my classmates, and my colleagues from whom I have learned a lot and who have been essential parts of my life, who have been helping me become not only a good student, but also a good person, a good friend.

Part I. The synthesis of n-type potassium-filled $IrSb_3$ skutterudite thermoelectric materials using K_3Sb precursor as compared to the synthesis using elemental potassium

Chapter 1. Introduction

Thermoelectric (TE) effects enable direct conversion between thermal and electrical energy. When a temperature gradient (ΔT) applied to a TE couple consisting of n-type and p-type elements, the mobile charge carriers diffuse from the hot end to the cold end, producing an electrostatic potential (ΔV). This phenomenon is known as the Seebeck effect (Figure 1a), where $\alpha = {}^{\Delta V}/_{\Delta T}$ is defined as the Seebeck coefficient, and is the basis for power generation.

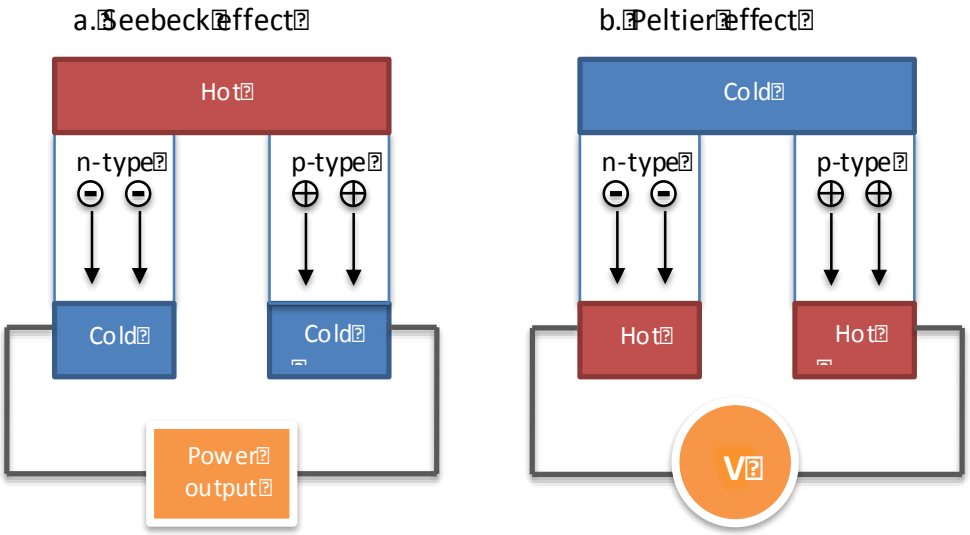

Figure 1. Schematic illustrations of a TE module for (a) power generation (Seebeck effect) and (b) active refrigeration (Peltier effect). (a) An applied temperature difference causes charge carriers in the material (electrons or holes) to diffuse from the hot side to the cold side, resulting in current flow through the circuit. (b) Heat evolves at the upper junction and is absorbed at the lower junction when a current is made to flow through the circuit.

Conversely, when a voltage is applied to a TE couple, the carriers flow through the circuit, which then causes the energy to be absorbed at one end and released at the other. This is known as the

Peltier effect (Figure 1b) and is the basis for electric refrigeration. In short, the TE effect can be used for both power generation and electric refrigeration.[1,2] Thermoelectric devices are solid-state devices, meaning they have no moving parts, and therefore are very reliable, making this technology attractive for many applications, including waste heat recovery and solar heat utilization (power generation) and temperature-controlled seats, portable picnic coolers and thermal management in microprocessors (electric refrigeration).[3]

The efficiency of TE devices is assessed by the dimensionless figure of merit (ZT):

$$ZT = \frac{\alpha^2}{\rho\kappa}T \qquad [1]$$

where α, ρ, κ, T are the Seebeck coefficient, the electrical resistivity, the total thermal conductivity and the absolute temperature.[4] A large Seebeck coefficient (corresponding to a large potential difference), low electrical resistivity (corresponding to low Joule heating), and low thermal conductivity (corresponding to a large temperature difference) are essential to obtain high performance TE materials. Two different research approaches have been studied in order to improve the efficiency of TE materials: one by exploring new materials with complex crystalline structures, and the other by reducing the dimension of the materials.

Several complex crystalline structures have been studied such as skutterudites, clathrates[5], Half-Heusler compounds[6], Zintl compounds[7] and so on. This thesis focuses on the structure of skutterudites, which possess a $CoAs_3$-type structure with the general chemical formula MX_3, where M is the transition-metal cobalt, rhodium or iridium, and X is phosphorus, arsenic or antimony.[8,9] This compound has a specific lattice structure composed of tilted octahedra of MX_3 which creates a large "cage'" located at the center of the unit cell, which could be filled with compatible metal atoms as shown in Figure 2.[10,11] Since the "cage" is sufficiently large, the fillers tend to "rattle" at their equilibrium position and therefore generate significant scattering of phonons.[12] Up until now, numerous investigations have been carried out on $CoSb_3$-based TE materials with respect to both doping strategies, filling strategies and synthesis processes, and several innovative results have been obtained.[13]

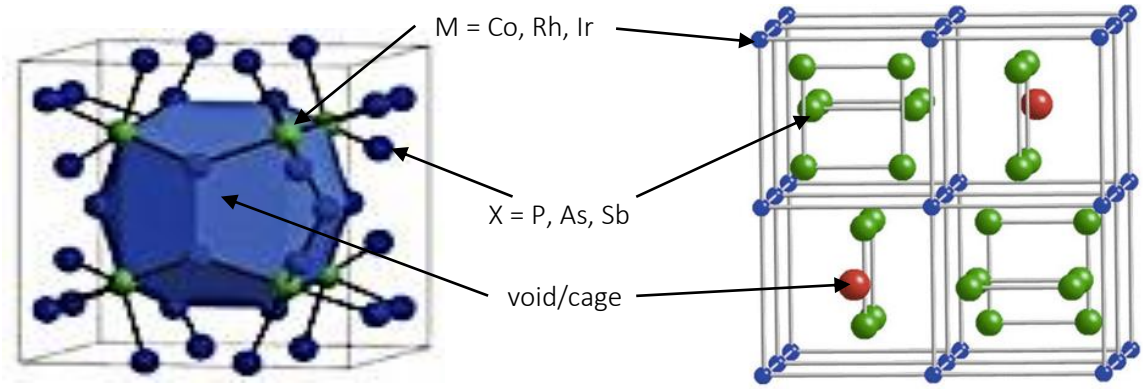

Figure 2. Two different views on the structure of skutterudites with substructure details. The figure on the left[10] shows the "cage" in the center of the structure formed by connecting octahedra of MX_3 (M = Co, Rh, Ir; X = P, As, Sb). The figure on the right[11] shows the whole unit cell consisting of eight cubes formed by M atoms; six of these cubes are filled with almost square planar rings of X_4 oriented as shown in the figures; two other cubes are left with voids, which can be filled by other metal atoms.

Filled skutterudites $A_yCo_4Sb_{12}$ have been a focus of research as typical "phonon-glass electron-crystal" materials proposed by Slack[14] for their promising thermoelectric efficiency. According to Shi *et al.*[15], the filling limit of filled skutterudites is related to the electronegativity difference between antimony and the filling element (R). Only the elements meeting the electronegativity difference condition of $\chi_{Sb} - \chi_R > 0.8$ can fill the "cage". A large number of research groups have studied the TE properties of filled $CoSb_3$ skutterudites with fillers varying among alkali metals (Na, K)[16], alkaline earth metals (Ca[17,18], Sr[19], Ba[20,21]), post-transition metals (In[22], Tl[23]), and rare earth metals (La, Ce, Nd, Eu, Yb).[24,25,26,27,28,29,30,31] $CoSb_3$ has been proven to be a very good choice for medium-temperature TE applications because both n- and p-type materials with high performance can be obtained in the same material system. In these filled skutterudites, the rattling motion of loosely bonded atoms within a large cage generates strong scattering effects against lattice phonon propagation; more advantageously, this "rattling" motion has less impact on the transport of electrons.[13] As a result, the thermal conductivity of skutterudites can be reduced significantly while preserving the electrical conductivity (or electrical resistivity) and the Seebeck coefficient, simply by doping and filling the voids with foreign atoms.[32,33]

Another focus of recent work in enhancing the ZT of skutterudite materials is reducing the grain sizes within the bulk material. In research on low-dimensional material systems, Dresselhaus *et al.*[34] suggested that the power factor (α^2/ρ) can be enhanced through the use of quantum confinement effects. As the system size decreases and approaches a nanometer length scale, the density of electronic states (DOS) can split and become narrow. Various low-dimensional systems, including superlattices, nanowires and quantum dots have been studied and shown promising results. However, for general applications, it is highly desirable to develop

high-performance bulk TE materials. Figure 3[35] shows the figure of merit of several typical TE materials as a function of time. As this figure has shown, ZT values can be improved significantly by the two methods mentioned above: filling the complex crystalline structure and nano-structuring.

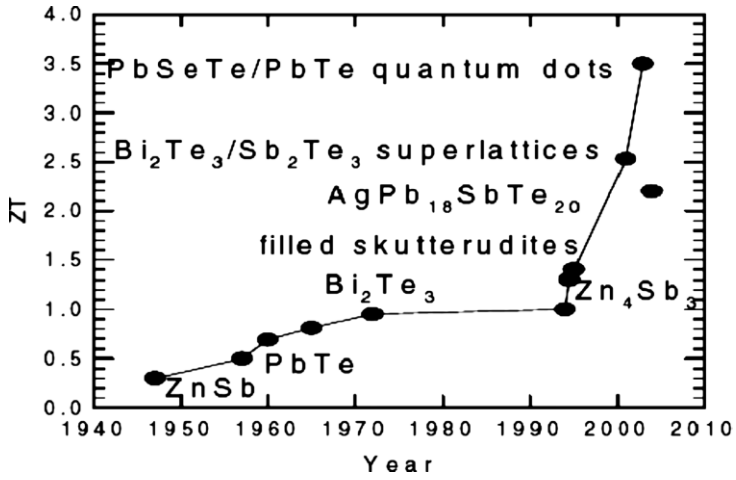

Figure 3. Figure of merit (ZT) of many typical thermoelectric materials as a function of time. The high performance of most of these materials is related to filling the complex structures and nanostructure engineering.

In the experiment presented here, the carrier concentration is the most important factor that is of concern because it can dominate the electronic transport behavior of the TE materials by exerting a significant effect on both the electrical conductivity and the Seebeck coefficient;[36] the electrical resistivity, the Seebeck coefficient and the thermal conductivity are mutually related and vary systematically as a function of carrier concentration.[37] It was also found that all TE properties depend closely on the carrier concentration and the optimal carrier concentration for typical TE materials was found to be in the range from 10^{19} to 10^{21} per cm^3.[38] In addition, the carrier concentration can be easily monitored by the level of doping or the filling fraction of the fillers, which can be initially estimated from the lattice parameter data calculated from X-ray

diffraction, and the materials' elemental composition obtained from scanning electron microscopy (SEM) and electron microprobe analysis (EPMA), respectively.

With promising results obtained from $CoSb_3$-based TE materials which can work efficiently throughout a mid-temperature range, $IrSb_3$ TE materials can operate at a higher maximum temperature. The peritectic decomposition of $IrSb_3$ occurs at 1136^0C (1409 K)[39], compared to 874^0C (1147 K) of $CoSb_3$[40]. Much work studying the filling fraction of $CoSb_3$ has been carried out and some results compiled in Figure 4[41] show the calculated and the experimental filling fraction limits for several fillers, which appear to be in strong agreement. There have been attempts on filling $IrSb_3$-based skutterudites with various metal fillers, but little work has been done to elucidate the maximum filling fraction achievable in $IrSb_3$ skutterudites.

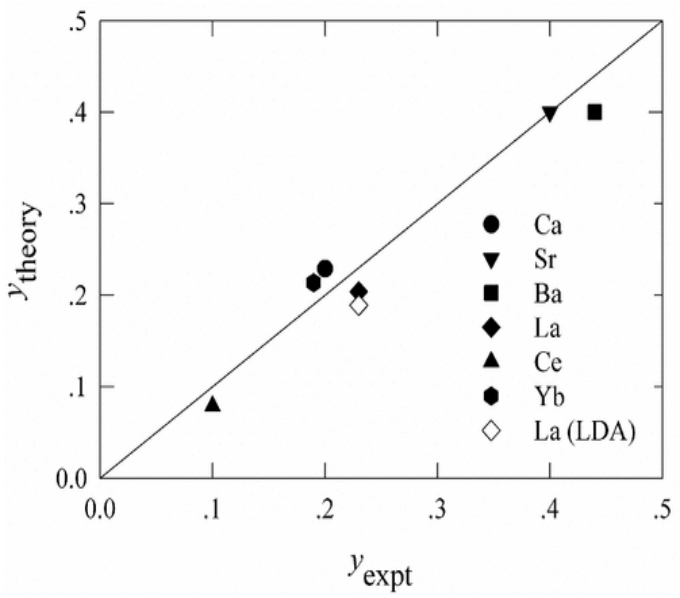

Figure 4. The theoretical and experimental maximum filling fractions of M-filled skutterudites, where M varies from alkali metals, alkaline earth metals and rare earth metals.

One of the more popular methods to synthesize skutterudites is ball milling stoichiometric amounts of elemental components, then reacting the homogenized powder in an

evacuated, sealed quartz tube, hot-pressing the resulting powder and ultimately forming the skutterudite structure. However, from past findings, the nominal filling fraction was significantly lower than the measured filling fraction. This discrepancy might be explained by the loss of starting materials, either by being oxidized or by being left behind on the walls of the ball mill vial, or possibly by the formation of unwanted secondary phases between the impurity filler elements and one of the other elements present.

For the purpose of simplicity in this experiment, potassium was chosen as the single filler since it satisfies the condition of electronegativity ($\chi_{Sb} - \chi_K > 0.8$); also, it is a one electron donor, removing additional uncertainty of multiple possible valence states of the filler atom. This ensures that the measured carrier concentration of the sample will likely be a good indication of how much of potassium was incorporated into the structure as a filler, relative to the nominal filling fraction.

An ultra-high filling fraction greater than 60% for potassium (K) in $CoSb_3$ is predicted by density functional calculations by Shi *et al.*[42] In 2006, Pei *et al.*[43] successfully synthesized potassium-filled $CoSb_3$, achieving a ZT of 1.0 at 800K in the compound $K_{0.38}Co_4Sb_{12}$ by a melting-quenching-annealing technique on highly pure starting materials including potassium, cobalt and antimony. In their experiment, they found a significant difference between the nominal filling fraction and the obtained filling fraction measured by EPMA. The main reason for the significant difference between the nominal and measured filling fractions is the considerable volatilization losses of K during the synthesis for the low melting point of about 880 K for the most likely secondary phase KSb, which is much lower than the annealing temperature. Pei *et al.* suggested that higher filling fractions may be obtained by using either low-temperature or high-pressure preparation methods.

Another reason for obtaining a lower than nominal filling fraction could be due to oxidation of starting materials. When elemental potassium was cut into small pieces in order to increase the surface to volume ratio to better homogenize the mixture, more surface oxidation of potassium could have occurred due to potassium's extremely high reactivity. Therefore, this work aimed to use a more stable precursor as a starting material as the source for potassium, measuring the effect that would have on filling efficiency. K_3Sb can be easily synthesized at a moderate temperature and then used in the subsequent step adding the remaining elements for the synthesis of potassium filled $K_yIr_4Sb_{12}$ skutterudite. The use of this precursor in lieu of elemental potassium should prevent some vaporization of potassium during the high temperature synthesis of $IrSb_3$ skutterudite due to the high vapor pressure of elemental potassium at low temperature (64^oC)[44].

Chapter 2. Experimental

2.1 Preparation of K_3Sb precursor

Due to the unique properties of potassium, hot-pressing the potassium can devitrify the quartz tube when potassium vaporizes at high temperature if a simple melting of the pure elements is carried out in a sealed, evacuated quartz tube. Therefore, in this experiment, stoichiometric amounts of elemental potassium (99.99%, pieces) and antimony (99.9999%, shot) (3:1) were put into a stainless steel vial for planetary ball milling in order to homogenize the mixture of the elements, milling the powder down to nanoparticles in order to obtain a high surface to volume ratio in the mixture. The vial was then heated at 90^0C for 48 hours in order to produce the K_3Sb precursor for the next step of the experiment.

2.2 Preparation of potassium filled cobalt-based skutterudites

Stoichiometric amounts of tripotassium antimonide (ball milled from the previous step, powder), antimony (99.999%, shot) and cobalt (99.99%, powder) were put into a stainless steel vial for ball milling in order to homogenize the mixture of reactants. The powder mixture was transferred into an evacuated quartz tube, then that tube was heated in a furnace at 750^0C for 48 hours to produce $K_yCo_4Sb_{12}$. After furnace treatment, the powder was then hot-pressed at 750^0C and 1.55 tons for 80 minutes to form a cylindrical pellet.

2.3 Preparation of potassium filled iridium-based skutterudites

Stoichiometric amounts of tripotassium antimonide (ball milled from the previous step, powder) and antimony (99.999%, shot) were put into a stainless steel vial for ball milling in order to homogenize the mixture of reactants. Elemental iridium (99.99%, powder) was then

added to the vial along with additional antimony. The powder was then hot-pressed according to the pressed profile listed in Table 1 to produce $K_yIr_4Sb_{12}$.

Table 1. Pressed Profiles of K-Filled Iridium-Based Skutterudite Samples

Sample	**Temperatures (^{0}C)**	**Time (minutes)**	**Force (tons)**
$K_{0.4}Ir_4Sb_{12}$	880	90	1.25
$K_{0.5}Ir_4Sb_{12}$ - low temp	800	60	1.00
$K_{0.5}Ir_4Sb_{12}$	880	90	1.25

2.4 Characterizations of potassium filled iridium-based skutterudites

The hot-pressed samples were then analyzed by X-ray diffraction (XRD) for phase purity and for lattice parameter calculations. Then, each sample was analyzed by scanning electron microscopy (SEM) and electron microprobe analysis (EPMA) to measure the phase purity and filling fraction from the images and measured elemental compositions, respectively. Thermoelectric properties of the samples were measured at the Jet Propulsion Laboratory in Pasadena, CA. The room temperature carrier concentration, carrier mobility, electrical resistivity, and Seebeck coefficient measurements were made. The heat capacity and thermal diffusivity were determined using a flash method[45]. Then, the thermal conductivity was calculated by $\kappa = \alpha D C_p$, where α, D, C_p are thermal diffusivity, density and heat capacity, respectively. The electrical resistivity and Hall effect were also measured using the van der Pauw technique.[46] The carrier concentration was calculated from the Hall coefficient by $^{p}/_{n} = {}^{1}/_{R_H e}$ where p and n are the densities of holes and electrons, and e is the electron charge. The Hall mobility (μ_H) was also calculated by $\mu = \frac{R_H}{\rho}$, where R_H is the Hall coefficient and ρ is the electrical resistivity. The

Seebeck coefficient were also measured on each sample between room temperature and approximately 750^0C (1023 K) using the light pulse technique[47]. The power factor was calculated by dividing the Seebeck coefficient squared by the electrical resistivity. Finally, the figure of merit for each sample at each temperature were also calculated by $ZT = \frac{\alpha^2}{\rho\kappa}T$, where α, ρ, κ, T are the Seebeck coefficient, the electrical resistivity, the thermal conductivity and the absolute temperature.

Chapter 3. Results and Discussion

3.1. The formation of K_3Sb precursor

Due to the highly air-sensitive properties of K_3Sb powder, the X-ray diffraction was not taken for the obtained precursor because it was difficult to obtain XRD without the proper inert environment XRD apparatus. However, after ball milling and warming of the vial for 48 hours, all of the sticky chunk of elemental potassium disappeared and only a homogeneous powder remained. This observation is consistent all of the potassium reacting with antimony to form the K_3Sb precursor.

3.2. Structural characterization of $K_yCo_4Sb_{12}$

The obtained pellet was fragile and appeared to be composed of multiple phases, even to the naked eye. However, Figure 4 shows that the X-ray diffraction pattern obtained from the hot-pressed pellet was in fact predominantly the structure of $CoSb_3$, with a small amount of some unknown impurities, possibly resulting from oxidized potassium that was unincorporated. The lattice parameter of the sample was calculated to be 9.044 ± 0.005 Å, compared to the referenced lattice parameter of unfilled $CoSb_3$ of 9.0385 Å. The increase in lattice parameter demonstrates that using the precursor resulted in successful potassium filling of the $CoSb_3$ structure. According to Pei *et al.*[43], the lattice parameters for $K_{0.3}Co_4Sb_{12}$ and $K_{0.6}Co_4Sb_{12}$ synthesized using elemental potassium were 9.042 ± 0.001 Å and 9.052 ± 0.001 Å, respectively. From the similarity in sizes between the $K_{0.4}Ir_4Sb_{12}$ sample made from the K_3Sb precursor and the $K_{0.3}Ir_4Sb_{12}$ sample made from elemental potassium from the literature, the synthesis of potassium-filled $CoSb_3$-based skutterudite utilizing elemental potassium ("K method") showed better filling efficiency than the synthesis utilizing the K_3Sb precursor ("K_3Sb method").

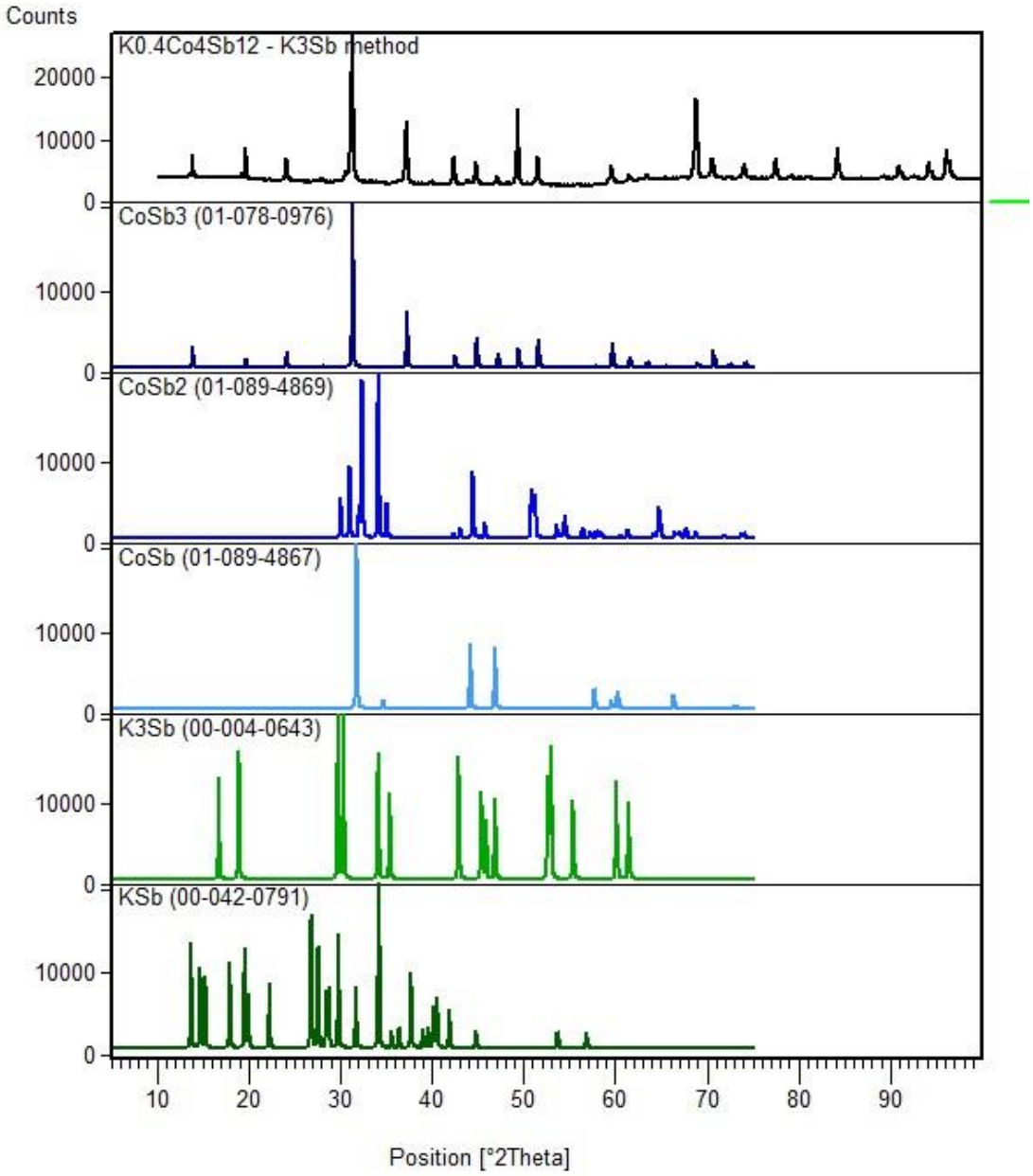

Figure 5. X-ray diffraction patterns of the hot-pressed $K_{0.4}Co_4Sb_{12}$. Simulated diffraction patterns generated from JCPDS reference patterns 01-078-0976 for $CoSb_3$, 03-089-4869 for $CoSb_2$, 01-089-4867 for CoSb, 00-004-0643 for K_3Sb, 00-042-0791 for KSb are included here for comparison to the experimental sample's pattern.

3.3. Structural characterization of $K_yIr_4Sb_{12}$

Figure 6 shows the X-ray diffraction patterns of the hot-pressed samples of $K_yIr_4Sb_{12}$ (y = 0.4, 0.5) made from the K_3Sb precursor (named as the K_3Sb method) compared to the $K_{0.5}Ir_4Sb_{12}$ sample made from elemental potassium (named as the K method). In order to determine the phase purity of each sample, the JCPDS reference pattern of $IrSb_3$ was included along with the reference patterns of the most likely secondary phases ($IrSb_2$, KSb). The reference pattern of the K_3Sb was also included in the figure in order to confirm that all of the K_3Sb precursor reacted and came into the skutterudite structure. The X-ray patterns confirm that the compound obtained possesses the structure of the $IrSb_3$ skutterudite, with a small amount of unknown impurities, which can be studied further in the SEM and EPMA analysis.

Figure 7 shows the cubic lattice parameters as a function of the filling fraction and Figure 8 shows the SEM images of the unfilled and potassium-filled $IrSb_3$ skutterudite samples. There were significant discrepancies between the nominal and EPMA-measured filling fractions. Furthermore, from the results, it was found that the samples made using the K_3Sb precursor showed lower filling efficiencies as compared to the skutterudite synthesis using elemental potassium. This might be because of the formation of impurities and secondary phases that we could not effectively identify in XRD. The SEM images of the $K_yIr_4Sb_{12}$ samples show the formation of significant amounts of impurities in rod-like shape and other random shapes. Table 2 shows the impurity percentage in each sample. Among the samples made using the K_3Sb precursor, the ones with higher filling fraction contained more impurities and among these samples, the one that was hot-pressed at lower temperature contained less impurities. This suggested that above 40% filling, the excessive fillers started to form secondary phases and exited the structure. However, by hot-pressing the sample at lower temperature undergoing a

smaller temperature gradient, more fillers can still be incorporated into the structure. The EPMA-measured filling fractions, the lattice parameters and the impurities percentages appear to agree well with each other.

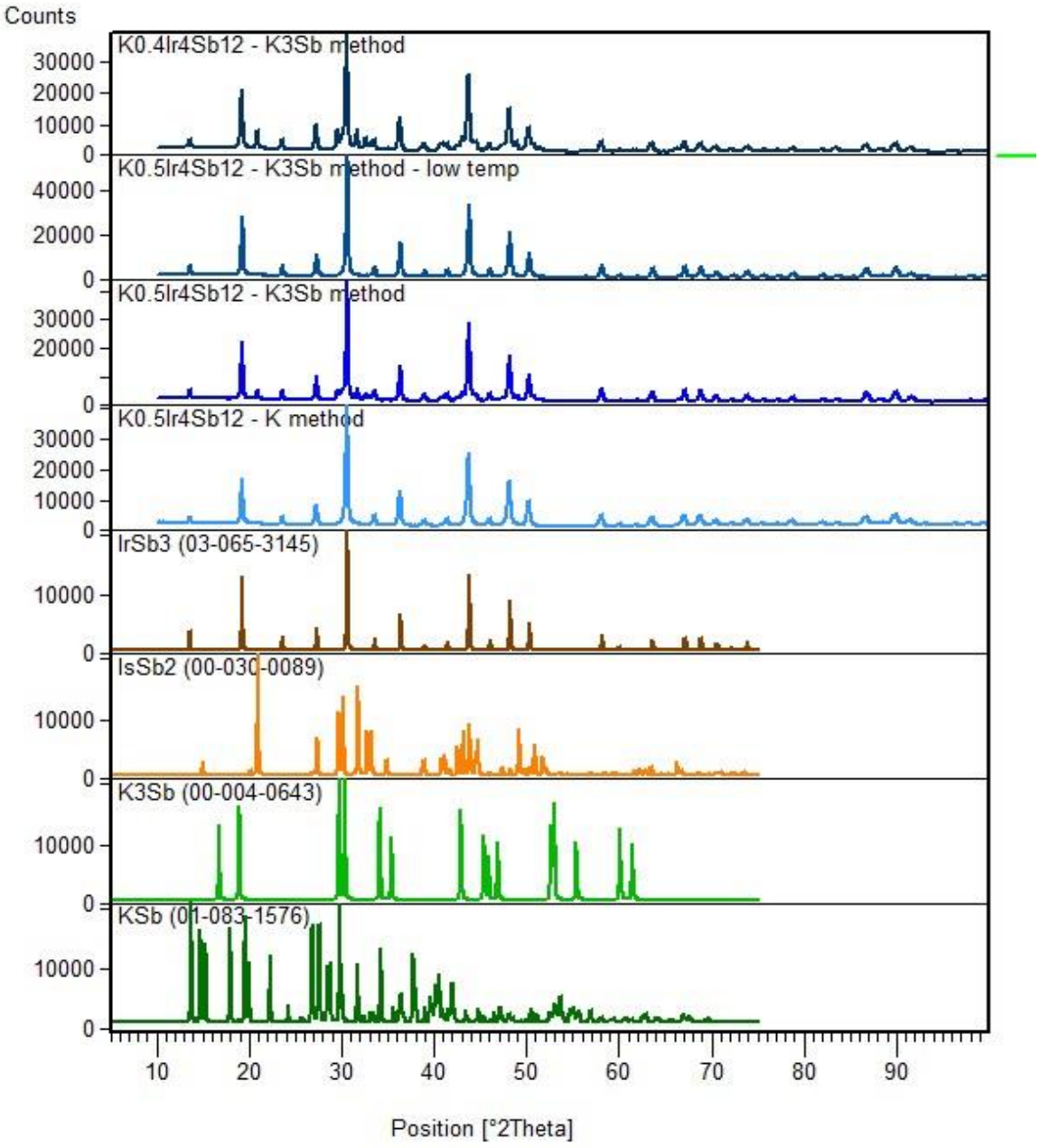

Figure 6: X-ray diffraction patterns of the hot-pressed samples. Simulated diffraction patterns generated from JCPDS reference patterns 03-065-3145 for $IrSb_3$, 00-030-0089 for $IrSb_2$, 00-004-0643 for K_3Sb, and 01-083-1576 for KSb are included here for comparison to the experimental samples' patterns.

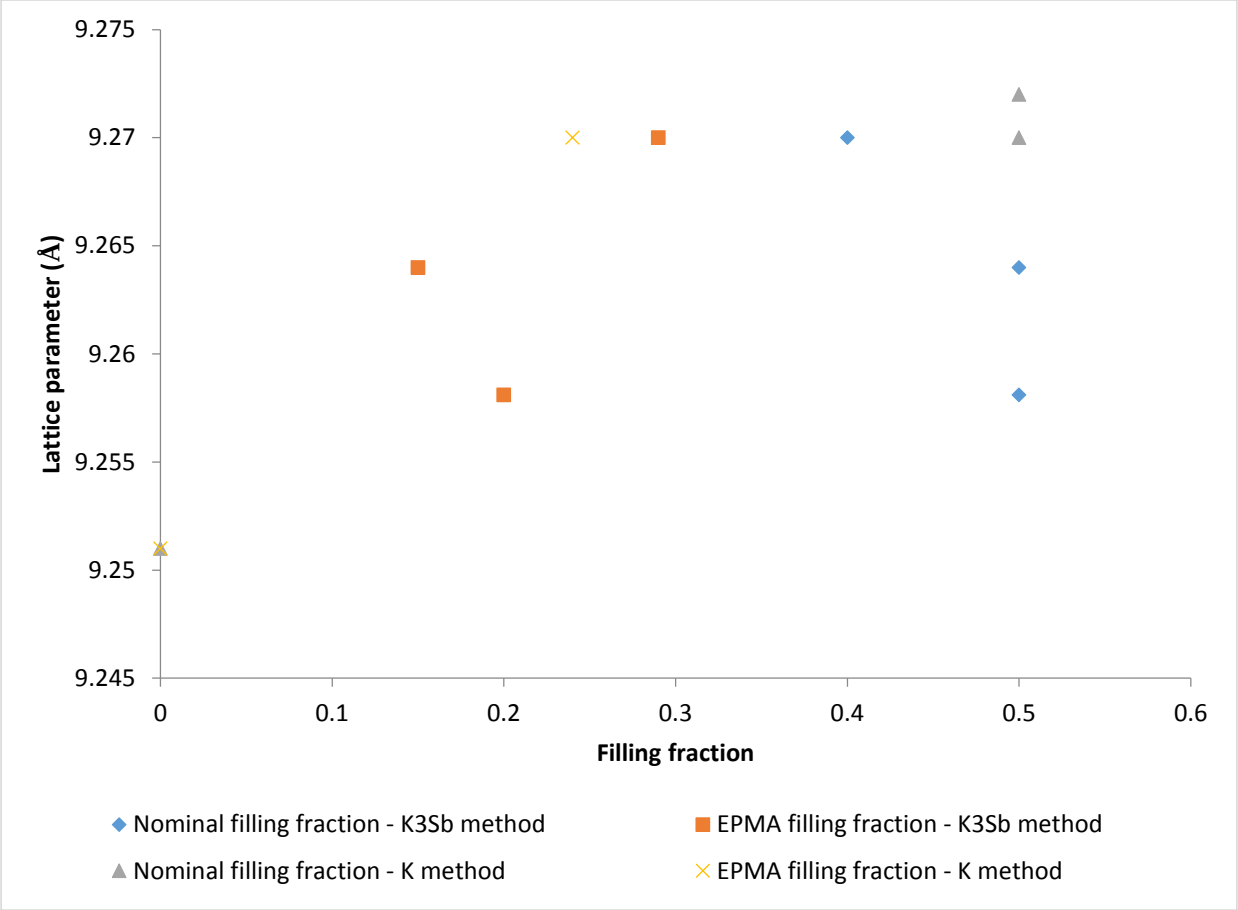

Figure 7. The lattice parameters against the nominal and the EPMA filling fraction of the $K_yIr_4Sb_{12}$ samples made by the traditional synthesis method and the proposed synthesis method.

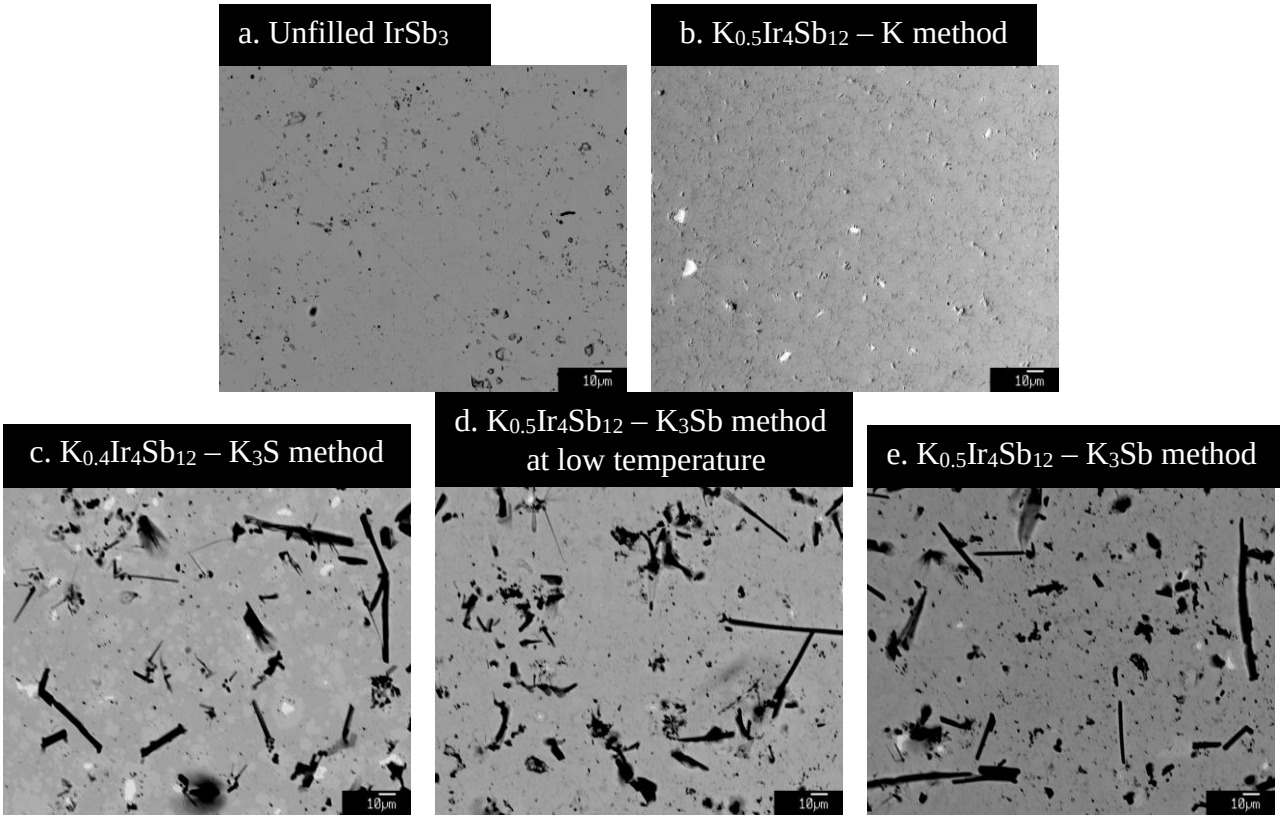

Figure 8. SEM image of the unfilled and K-filled $IrSb_3$ skutterudite samples.

a. Unfilled $IrSb_3$; b. $K_{0.5}Ir_4Sb_{12}$ sample made from elemental potassium; c. $K_{0.4}Ir_4Sb_{12}$ sample made from the K_3Sb precursor; d. $K_{0.5}Ir_4Sb_{12}$ samples made from the K_3Sb precursor, hot-pressed at 800^0C and under a lower initial temperature gradient; e. $K_{0.5}Ir_4Sb_{12}$ samples made from K_3Sb precursor, hot-pressed at 880^0C.

Table 2. Impurity Percentages in Unfilled and Potassium-Filled $IrSb_3$ Skutterudite Samples

Sample	**% impurities***
unfilled $IrSb_3$	17.33
$K_{0.5}Ir_4Sb_{12}$ – K method	0.636
$K_{0.4}Ir_4Sb_{12}$ – K_3Sb method	36.83
$K_{0.5}Ir_4Sb_{12}$ – K_3Sb method – low temperature	35.99
$K_{0.5}Ir_4Sb_{12}$ – K_3Sb method	50.03

*The impurities were totaled from both bright spots and dark spots in the SEM images.

3.4. Thermoelectric properties of $K_yIr_4Sb_{12}$

The room temperature electrical properties, carrier concentration and mobility for different samples are listed in Table 3. The values from the table are graphed in Figure 9. The carrier concentrations of the potassium-filled samples do not show a linear correlation between the carrier concentration and the lattice parameter, which is reasonable since with higher filling fractions (higher lattice parameter), more secondary carriers are present and this therefore decreases the absolute carrier concentration. However, it is safe to conclude that as the lattice parameter increases (corresponding with higher EPMA filling fractions), the carrier concentration increases. Furthermore, the absolute carrier mobility decreases slightly as the lattice parameter increases.

Figure 10 presents the carrier concentration as a function of temperature ranging from room temperature to about 1023 K for potassium-filled $IrSb_3$ samples. As the figure shows, the carrier concentration varies significantly among the samples. Samples with higher lattice parameters (higher EPMA filling fraction) show higher initial carrier concentrations at room temperature. At high temperature, more carriers are activated until the minority carriers dominate. The temperature at which the carrier concentration reaches its highest value varies significantly among samples; for example, for the sample "$K_{0.5}Ir_4Sb_{12}$ – K method", the maximum carrier concentration is about $2.3x10^{21}$ cm^{-3} at about 790 K, while the maximum carrier concentration of "$K_{0.5}Ir_4Sb_{12}$ – K_3Sb method" is about $1.0x10^{21}$ cm^{-3} at about 670 K, and of "$K_{0.5}Ir_4Sb_{12}$ – K_3Sb method – low temp." is about $9.0x10^{20}$ cm^{-3} at about 590 K. This huge variation suggests that different filling fractions cause drastic changes in the carrier concentration and the temperature at which it is activated.

Figure 11 plots the carrier mobility as a function of temperature for the $K_yIr_4Sb_{12}$ samples. Undoped $IrSb_3$ shows significantly higher mobility at all temperatures, and therefore is plotted separately in the inset of the figure. This is probably because the carriers are scattered at the grain boundaries due to doping, in which the filler partially disrupts the crystalline structure compared to the undisrupted p-type undoped structure. In addition, the mobility of the undoped sample decreases as the temperature increases, while the doped samples show the opposite trend: their mobility increases as the temperature increases. The measured mobilities at high temperatures for the filled n-type samples indicate that the minority carriers begin to dominate at higher temperatures.

The electrical resistivity as a function of temperature for $K_yIr_4Sb_{12}$ samples is presented in Figure 12. Resistivity decreases with increasing lattice parameters as shown in Figure 9. This agrees with the assumption that the filler atoms contribute more n-type charge carriers to the structure from the filler atoms as the filling fraction increases, which also causes the lattice parameter to increase. The resistivity of the sample synthesized with elemental potassium increases slightly as the temperature increases, while the samples synthesized using K_3Sb has significantly higher electrical resistivity, compared to the samples using elemental potassium. At higher temperature, the resistivities of the samples decrease and converge as the carriers from the donor atoms of the filled n-type samples become less significant compared to the thermally generated carriers.

Figure 13 shows the plot of Seebeck coefficient as a function of temperature for $K_yIr_4Sb_{12}$ samples. The undoped sample is a p-type material with a positive Seebeck coefficient, while the doped samples definitely show n-type characteristics. As with the temperature dependence of electrical resistivity, the Seebeck coefficient differs significantly among samples. At room

temperature, the Seebeck coefficient of the greatest magnitude was obtained from the $K_{0.5}Ir_4Sb_{12}$ sample prepared using the K_3Sb synthesis method. However, at high temperature, the magnitude of the Seebeck coefficient for this sample also decreases at a faster rate than that of the sample using elemental potassium. The samples prepared using the K_3Sb method each had Seebeck coefficients of lower magnitudes at 1023 K, as compared to the sample prepared using elemental potassium. The Seebeck coefficient of the greatest magnitude at 1023 K was obtained from the $K_{0.5}Ir_4Sb_{12}$ – K method sample, which also had the highest lattice parameter, indicating that the sample also had the greatest amount of potassium filling in the structure. Filling fractions of the doped samples, measured by EPMA also agree with this trend.

The total thermal conductivity as a function of temperature is plotted in Figure 14. The thermal conductivity of the doped samples is significantly lower than the thermal conductivity of the undoped sample, supporting the assumption that the filler atoms effect phonon scattering in the structure, thereby reducing the total thermal conductivity of the sample. Furthermore, the thermal conductivity decreases as the lattice parameter and EPMA filling fractions increase. The $K_{0.5}Ir_4Sb_{12}$ – K method sample – had the lowest thermal conductivity at all temperatures measured. The lattice contribution to the total thermal conductivities were calculated for each individual sample and plotted in Figure 15. By comparing the values of total thermal conductivity and lattice thermal conductivity, the electronic contribution to the thermal conductivity appears to be dominated by the lattice contribution. Just as with the total thermal conductivity, the lattice contribution of the thermal conductivity follows the same trend as the total thermal conductivity. Additionally, the room temperature lattice thermal conductivities decrease as the lattice parameters and the EPMA measured filling fractions increase, and these values start to converge at high temperature.

The power factors (α^2/ρ) are measured and plotted in Figure 16. From all of the above TE properties, the one that seems to be responsible for this inefficiency is the contribution of the electrical resistivity. Even though the doped samples have higher Seebeck coefficients and lower thermal conductivites than the undoped sample, their resistivities are also significantly higher than the undoped sample. However, when comparing the power factors among the doped samples, the power factors seem to be higher for the sample with the higher lattice parameter and higher EPMA filling fraction. Therefore, although potassium is not a beneficial filler for improving the thermoelectric properties of the $IrSb_3$ skutterudites, among the filled samples, the filling fraction still provides a positive role in improving the power factor.

The dimensionless figure of merit ZT is calculated for each sample and shown in Figure 17. Peak ZT values for each potassium filled sample occur between 600-750 K. ZT values appear to increase with filling fractions and lattice parameters.

Table 3. Room Temperature Lattice Parameters (a), Carrier Concentrations (n/p), Mobilities (μ), Electrical Resistivites (ρ) and Seebeck Coefficients (α) for $K_yIr_4Sb_{12}$ Samples

y (nominal)	**y (EPMA)**	**a (Å)**	**Absolute Carrier Concentration n/p (cm^{-3})**	**Carrier Mobility ($cm^2/V.s$)**	**Resistivity (mΩ.cm)**	**Seebeck coefficient (μV/K)**
0	0	9.250	1.71E+19	1022.21	0.3584	27.3
0.5	0.24	9.270	2.27E+20	6.149067	4.48096	-92.7
0.4	0.29	9.270	1.08E+20	8.496438	6.8229	-84.7
0.5	0.20	9.258	3.30E+19	8.713654	21.6890	-130
0.5	0.15	9.264	4.32E+19	9.591459	15.0778	-126.9

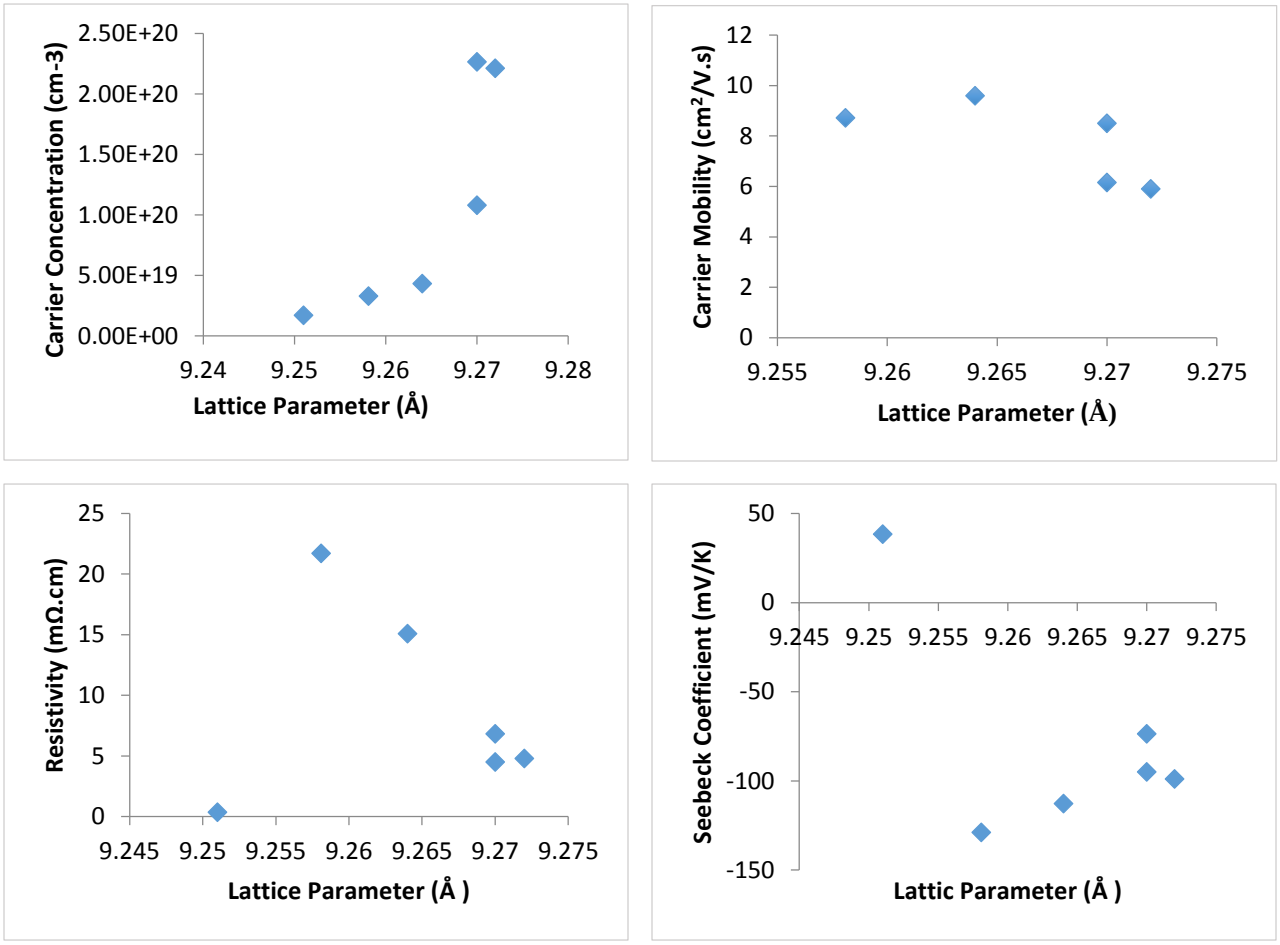

Figure 9. The carrier concentration, mobility, resistivity and estimated Seebeck coefficient at room temperature against cubic lattice parameter for $K_yIr_4Sb_{12}$ samples.

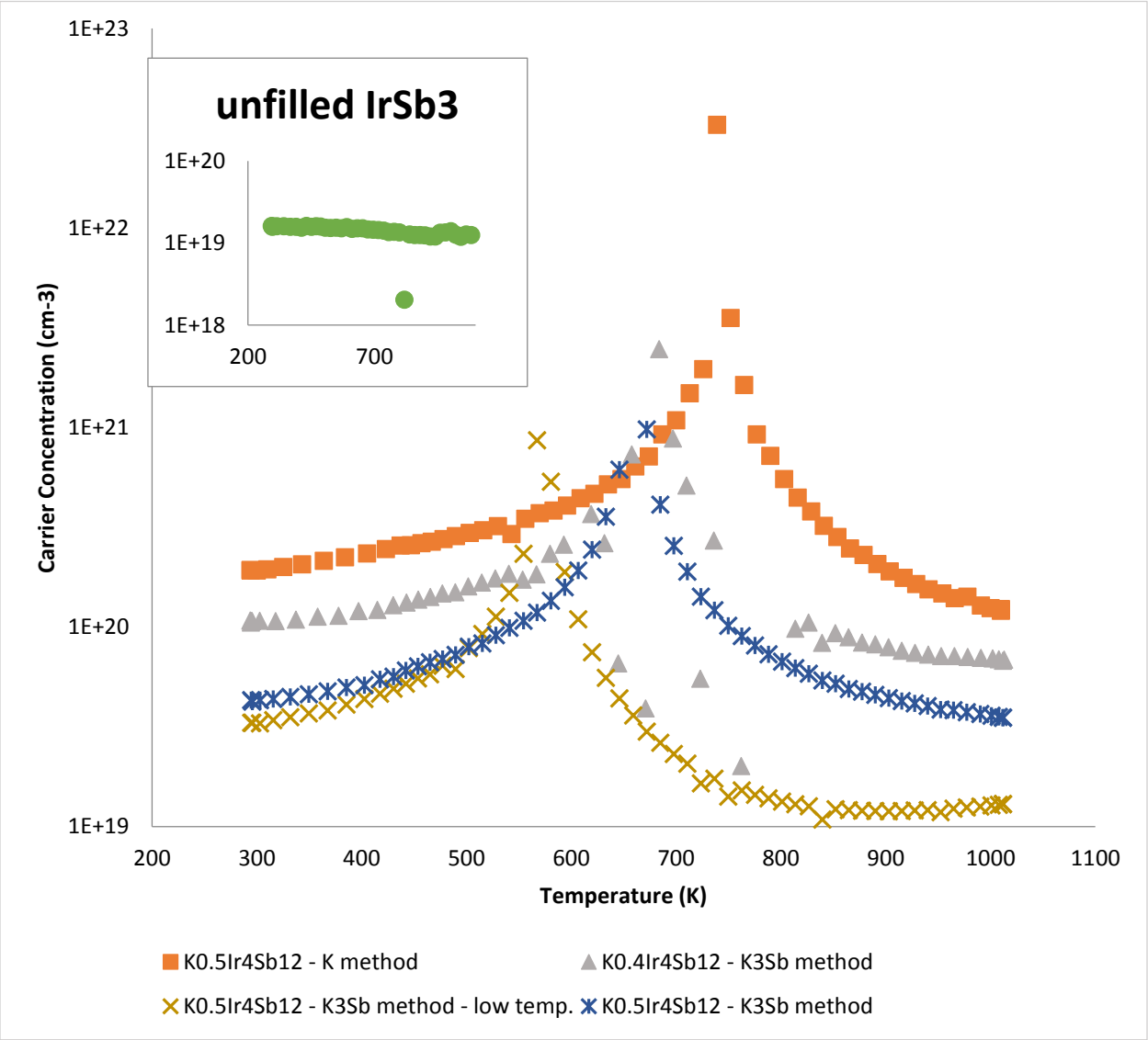

Figure 10. Carrier concentration of $K_yIr_4Sb_{12}$ samples as a function of temperature. The inset shows the significantly smaller carrier concentration of the unfilled $IrSb_3$ sample as a function of temperature. The carrier concentration is calculated by $^{p}/_{n} = {}^{1}/_{R_H e}$, where p and n are the densities of holes and electrons, e is the electron charge, and R_H is the Hall coefficient measured by the light pulse technique.

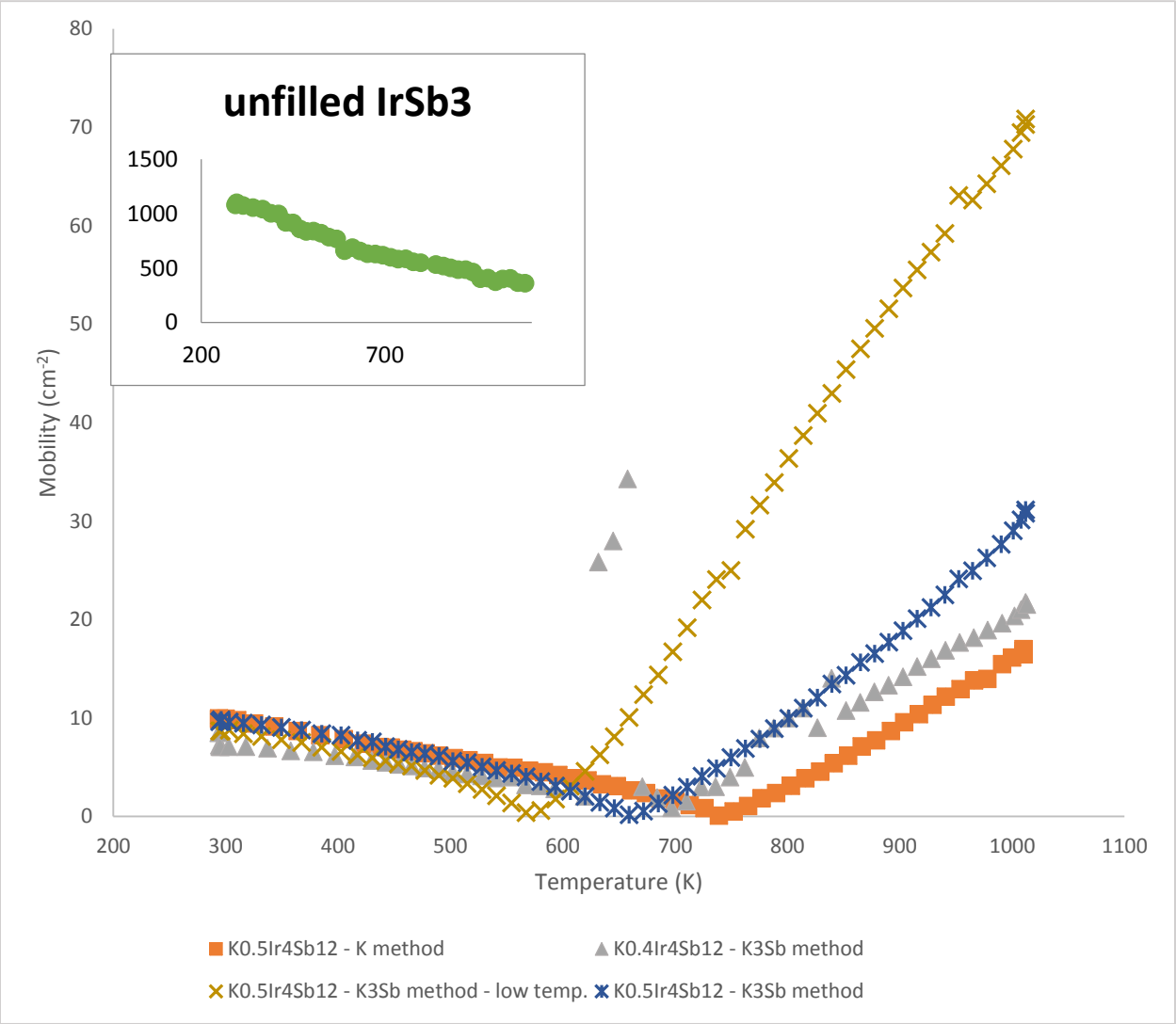

Figure 11. Mobility of $K_yIr_4Sb_{12}$ samples as a function of temperature. The inset shows the significantly higher carrier mobility of the unfilled $IrSb_3$ sample as a function of temperature. The Hall mobility was calculated by $\mu = \frac{R_H}{\rho}$, where R_H is the Hall coefficient and ρ is the electrical resistivity.

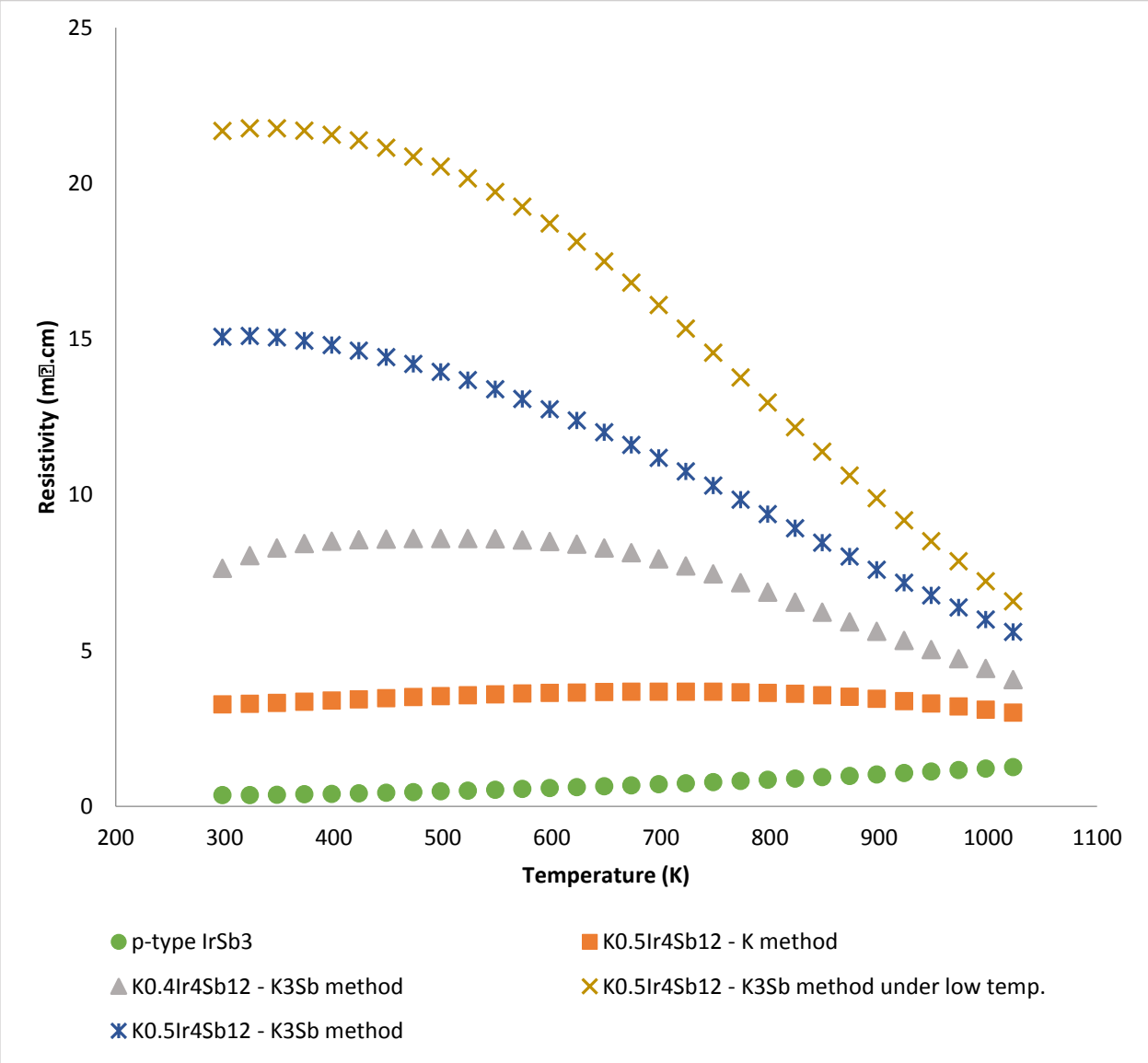

Figure 12. Electrical resistivity (ρ) as a function of temperature in the $K_yIr_4Sb_{12}$ samples. Electrical resistivity was measured using the van der Pauw technique.

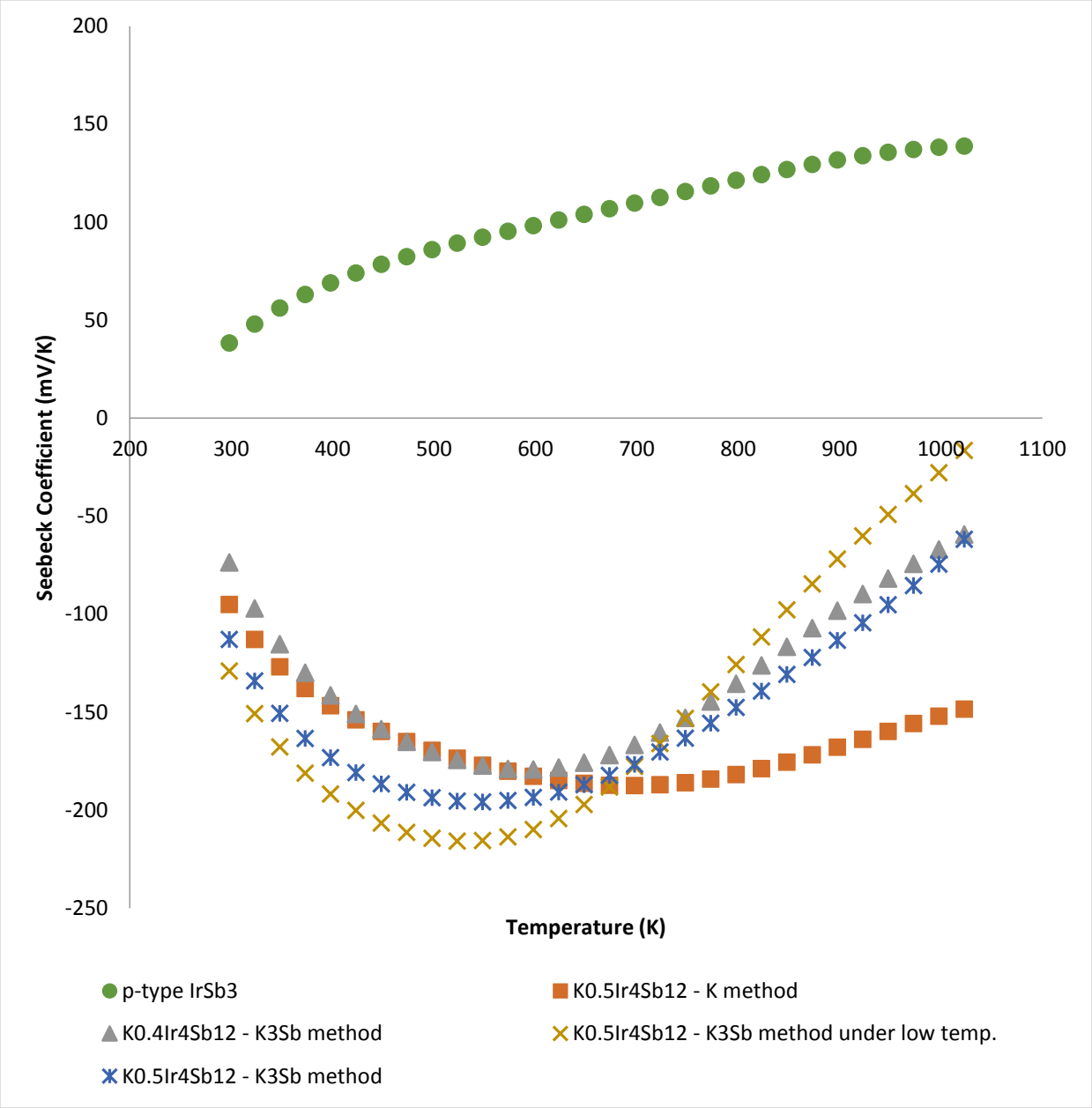

Figure 13. Seebeck coefficient as a function of temperature in the $K_yIr_4Sb_{12}$ samples. The Seebeck coefficient was measured using the light pulse technique.

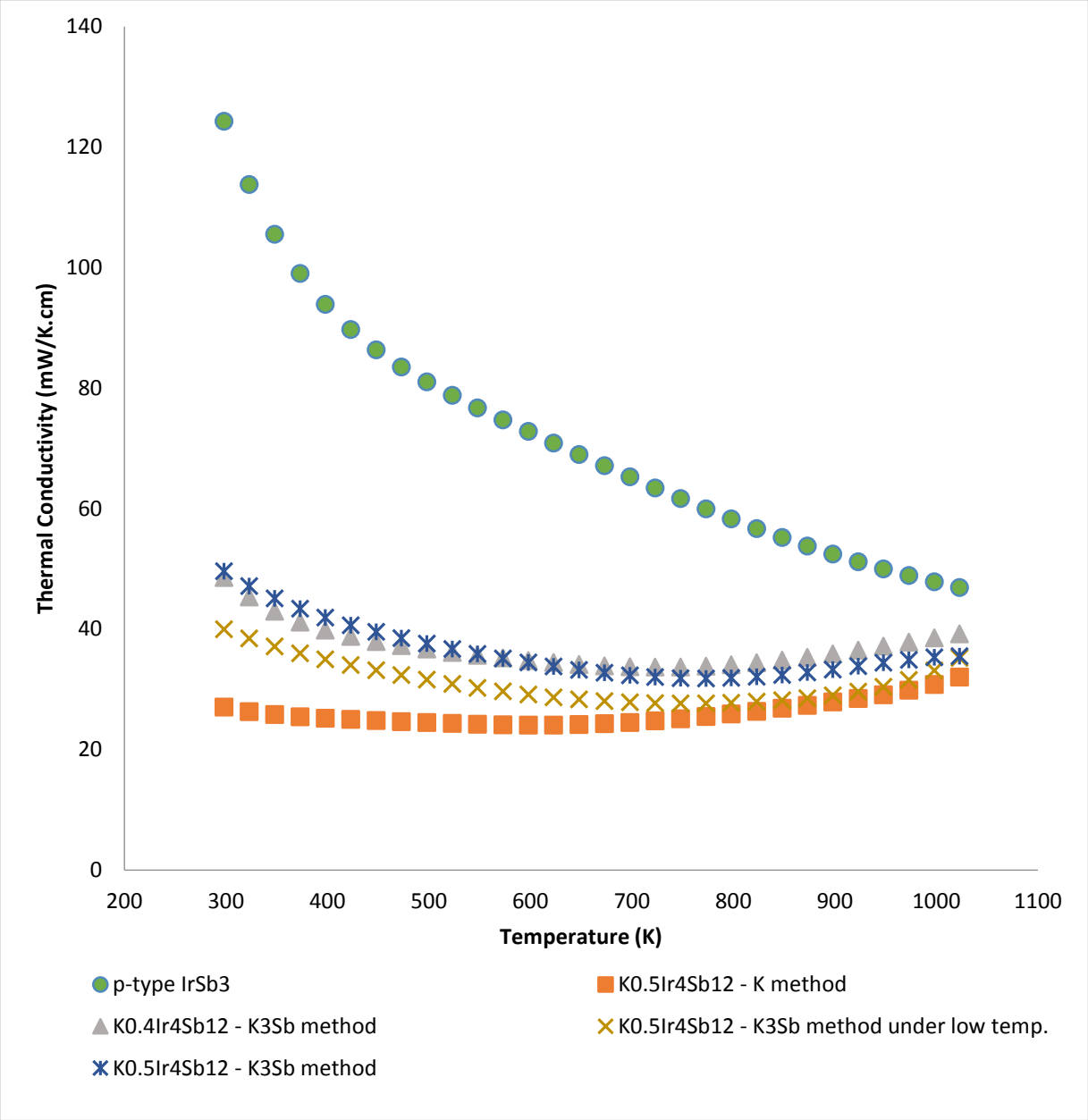

Figure 14. The total thermal conductivity as a function of temperature in the $K_yIr_4Sb_{12}$ samples. The total thermal conductivity was calculated using the flash method.

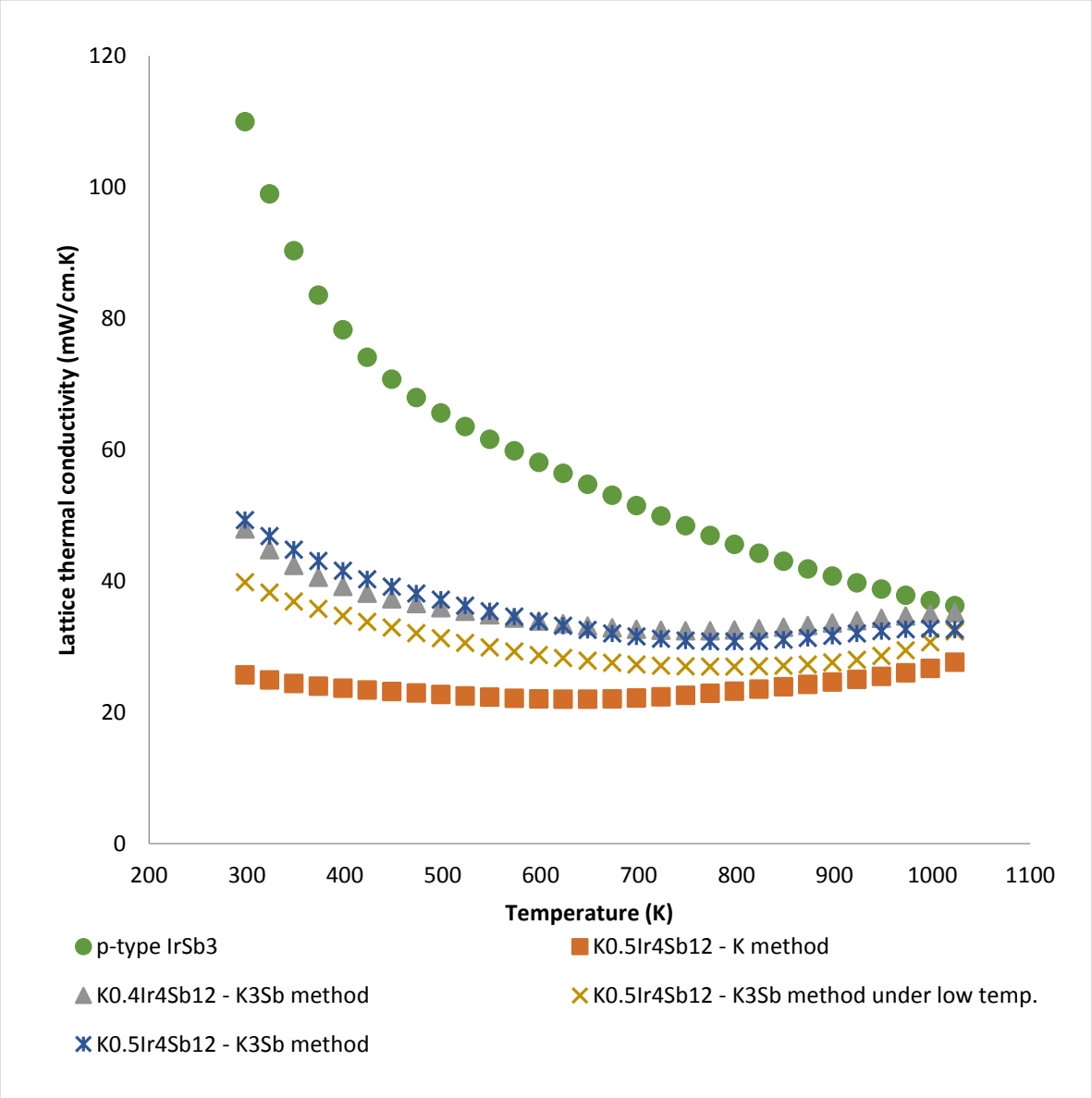

Figure 15. Lattice thermal conductivity (κ_L) as a function of temperature in the $K_yIr_4Sb_{12}$ samples. The lattice thermal conductivity was obtained by subtracting the electronic thermal conductivity from the total thermal conductivity. The electronic thermal conductivity was calculated using the Widemann-Franz law $K_e\rho = LT$, where ρ is the electrical resistivity, L is Lorenz number which is equal to $2.44 \times 10^{-8} W\Omega K^{-2}$ and T is the absolute temperature.

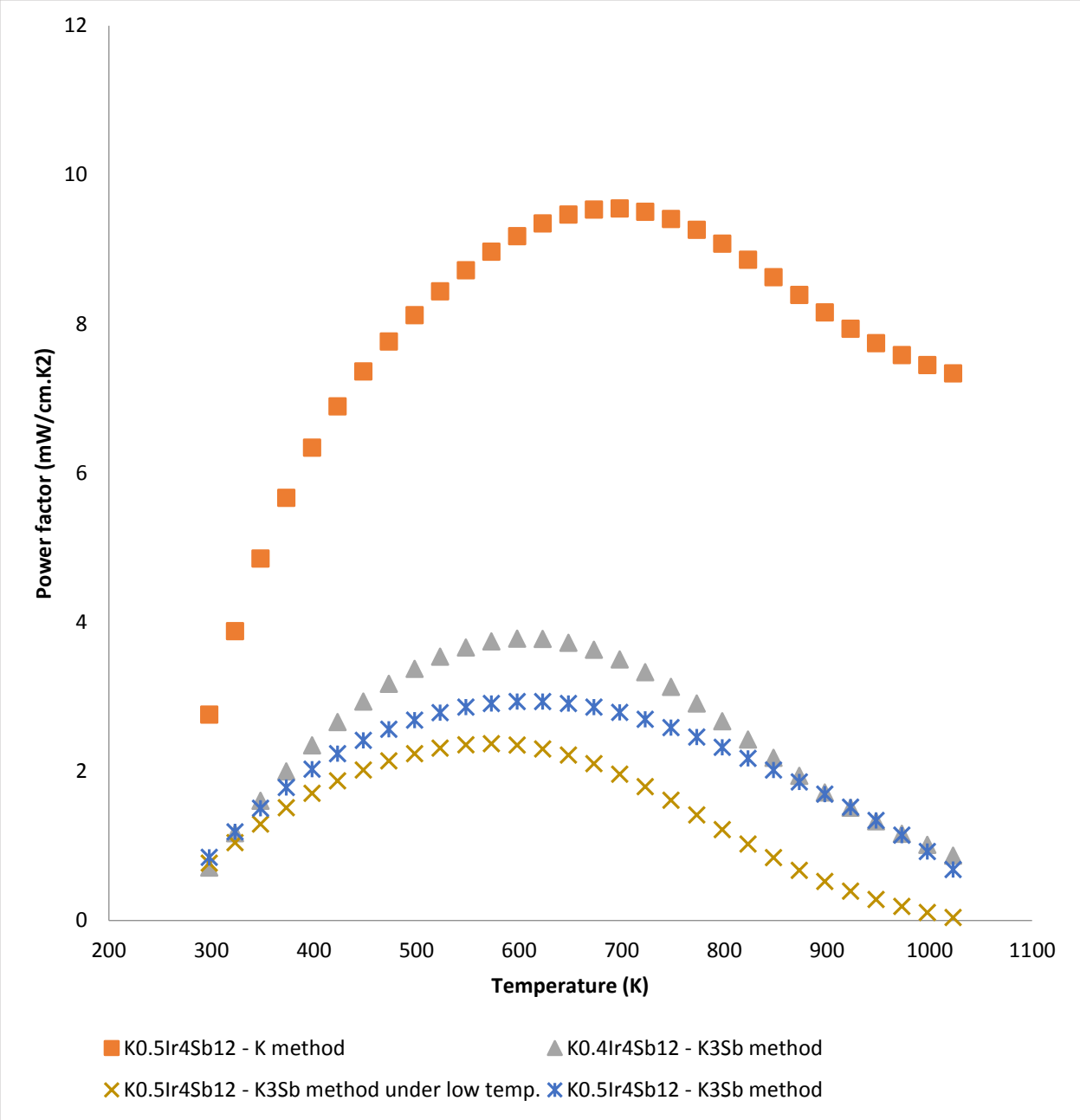

Figure 16. The power factors (α^2/ρ) as a function of temperature in the $K_yIr_3Sb_{12}$ samples.

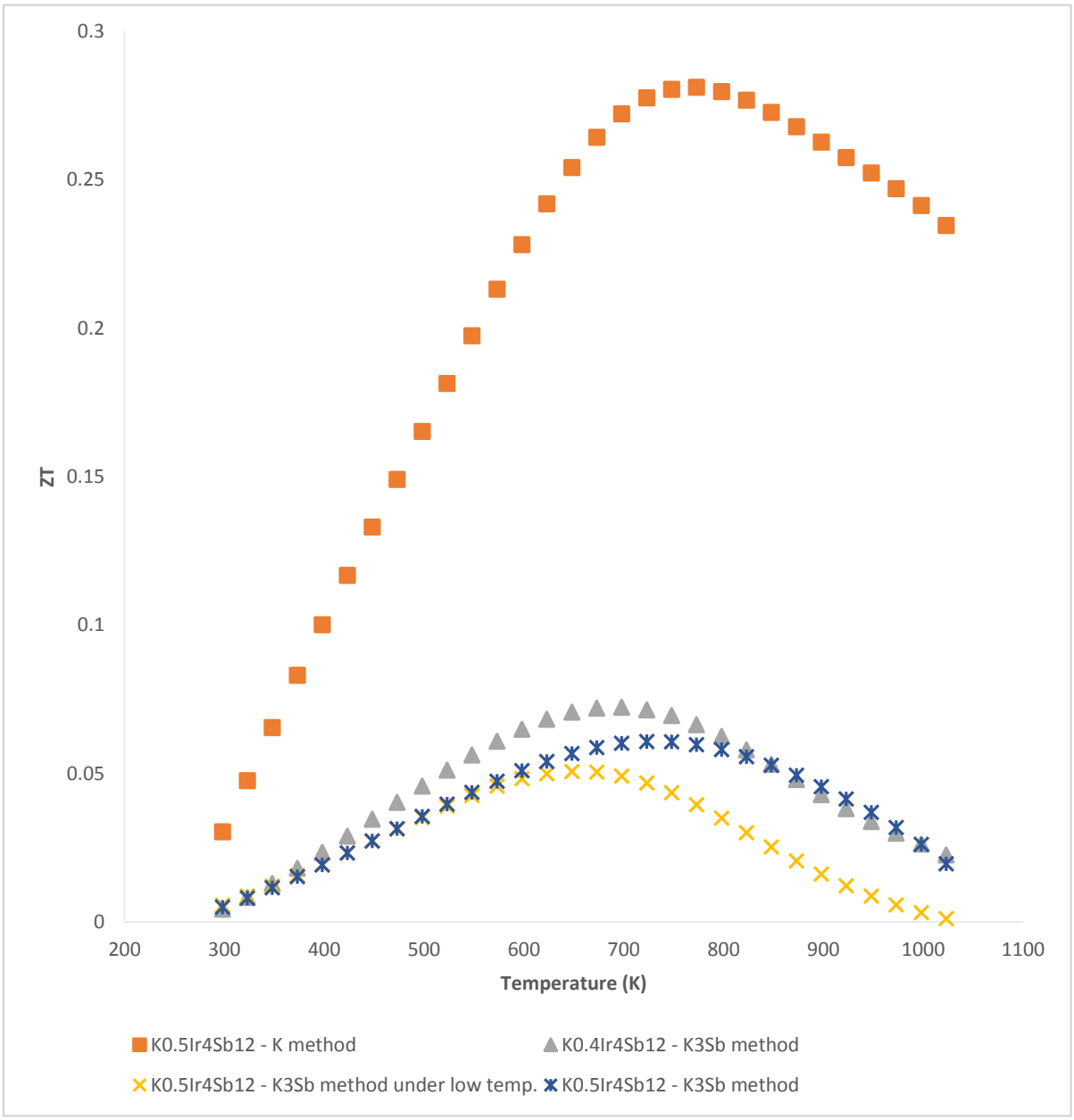

Figure 17. The figure of merit (ZT) as a function of temperature in the $K_yIr_4Sb_{12}$ samples. The figure of merit was calculated by $ZT = \frac{\alpha^2}{\rho\kappa}T$, where α is the Seebeck coefficient, ρ is the electrical resistivity, κ is the total thermal conductivity and T is the absolute temperature.

Chapter 4. Conclusions

The synthesis of n-type potassium filled skutterudite thermoelectric materials using K_3Sb as a precursor has been demonstrated along with the synthesis method using elemental potassium. The final samples were characterized by X-ray diffraction (XRD), scanning electron microscopy (SEM), electron microprobe analysis (EPMA), and thermoelectric (TE) properties. The "K_3Sb method" was found to be less effective than the "elemental K method". The EPMA and SEM data suggest the presence of an undesired phase impurity, other than that of $IrSb_2$, which was present elsewhere. The highest ZT among the $K_yIr_4Sb_{12}$ samples was found to be 0.28 at 500^0C (773 K). Potassium proved to be an effective filler, best incorporated when added as elemental potassium in the synthesis of filled, n-type, iridium-based skutterudite. ZT values obtained for these filled samples represent a significant improvement over all others reported in the literature for n-type $IrSb_3$ skutterudite, and this work addresses concerns about limiting the reactivity of highly reactive, elemental filler atoms during skutterudite synthesis by pre-reacting elemental filler atoms with antimony.

References

(1) Li, Jing-Feng, Wei-Shu Liu, Li-Dong Zhao, Zin Zhou, *NPG Asia Mater.*, **2010**, *2(4)*, 152-158.

(2) Riffat, S.B., X. Ma, "Thermoelectrics: a review of present and potential applications", *Appl. Therm. Eng.*, **2003**, *23*, 913-935.

(3) Bell, L.E., *Science*, **2008**, *321*, 1457-1461.

(4) Liu, W.S., L.D. Zhao, B.P. Zhang, J.F. Li, *Applied Physics Letters*, **2008**, *93*, 042109.

(5) Takabatake, Toshiro, K. Suekuni, T. Nakayama, E, Kaneshita, "Phonon-glass electron-crystal thermoelectric clathrates: Experiments and theory", *Reviews of Modern Physics*, **2014**, *86*, 669-716

(6) Nolas, G.S, J. Poon, M. Kanatzidis, "Recent developments in bulk thermoelectric materials", *MRS Bulletin*, **2006**, *31*, 199-205.

(7) Kauzlarich, S.M., S.R. Brown, G.J. Snyder, "Zintl phases for thermoelectric devices", *Dalton Trans.*, **2007**, 1099-2107.

(8) Uher, C., "Recent Trends in Thermoelectric Material Search I", *Semiconductors and Semimetals*, T.T. Tritt. Ed., **2001**, *69*.

(9) Berardan, D. *et al.*, *Journals of Applied Physics*, **2005**, *98*, 033710.

(10) Snyder, G.J., E.S. Toberer, "Complex thermoelectric materials", *Nature Materials*, **2008,** *7*, 104-114.

(11) Kurosaki, Ken, A. Harnwinggmoung, S. Yamanaka, "Thermoelectric Properties of $CoSb_3$ Based Skutterudites Filled by Group 13 Elements", *Nanoscale Thermoelectrics SE - 10*, **2014**, 301-325.

(12) Slack, G.A., *CRC Handbook of Thermoelectrics*, D.M. Rowe ed., *CRC Press,* **1995**, Chap. 34, 407.

(13) Shi, Xun, S.Q. Bai, L.L. Xi, J. Yang, W.Q. Zhang, L.D. Chen, J.H. Yang, "Realization of high thermoelectric performance in n-type partially filled skutterudites", *Journal of Materials Research*, **2011**, *26 (15)*, 1745-1754.

(14) Slack, G.A, *CRC Handbook of Thermoelectrics*, D.M. Rowe, ed., *CRC Press*, **1995**, *34*, 407.

(15) Shi, X., W. Zhang, L.D. Chen, J. Yang, *Physics Review Letters*, **2005**, *95*, 185503.

(16) Mei, Z.G., J. Yang, Y.Z. Pei, W. Zhang, L.D. Chen, "Alkali-metal-filled $CoSb_3$ skutterudites as thermoelectric materials: Theoretical study", *Physical Review B.*, **2008**, *77(4)*, 045202(8).

(17) Puyet, M., B. Lenoir, A. Dauscher, M. Dehmas, C. Stiewe, E. Muller, *J. Appl. Phys.*, **2004**, *95*, 4852-4855.

(18) Puyet, M., A. Dauscher, B. Lenoir, M. Dehmas, C. Stiewe, E. Muller, J. Hejtmanek, *J. Appl. Phys.*, **2005**, *97*, 083712(4).

(19) Zhao, X.Y., X. Shi, L.D. Chen, W.Q. Zhang, W.B. Zhang, Y.Z. Pei, *J. Appl. Phys.*, **2006**, *99*, 053711(4).

(20) Chen, L.D., T. Kawahara, X.F. Tang, T. Goto, *J. Appl. Phys.*, **2001**, *90(4)*, 1864-1868.

(21) Dyck, J.S., W. Chen, C. Uher, L.D. Chen, X.F. Tang, T. Hirai, *J. Appl. Phys.*, **2002**, *91*, 3698-3905.

(22) He, Tao, J.Z. Chen, H.D. Rosenfeld, M.A. Subramanian, "Thermoelectric properties of Indium-filled skutterudites", *Chem. Mater.*, **2006**, *18(3)*, 759-762.

(23) Sales, B.C, B.C Chakoumakos, D. Mandrus, "Thermoelectric properties of thallium-filled skutterudites", *Phys. Rev. B.*, **2000**, *61*, 2475-2481.

(24) Nolas, G.S., J.L. Cohn, G.A. Slack, "Effect of partial void filling on the lattice thermal conductivity of skytterudites", *Physics Review B.*, **1998**, *58(1)*, 164-170.

(25) Gajewski, D., N.R. Dilley, E.D. Bauer, E.F. Freeman, R. Chau, M.B Maple, D. Mandrus, B.C. Sales, A.H. Lacerda, "Heavy fermion behavior of the cerium-filled skutterudites $CeFe_4Sb_{12}$ and $Ce_{0.9}Fe_3CoSb_{12}$", *J. Phys.:Condens. Matter*, **1998**, *10*, 6973-6985.

(26) Sales, B.C., D. Mandrus, R.K. Williams, "Filled skutterudites antimonies: A new class of thermoelectric materials", *Science*, **1996**, *272(5266)*, 1325-1328.

(27) Kuznetsov, V.L., L.A. Kuznetsova, D.M. Rowe, "Effect of partial void filling on the transport properties of $Nd_xCo_3Sb_{12}$ skutterudites", *J. Phys.: Condens. Matter*, **2003**, *15*, 5035-5048.

(28) Lamberton Jr., G.A., S. Bhattacharya, R.T. Littleton IV, M.A. Kaeser, R.H. Tedstrom, T.M. Tritt, J. Yang, G.S. Nolas, "High figure of merit in Eu-filled $CoSb_3$-based skutterudites", *Appl. Phys. Lett.*, **2002**, *80*, 598-600.

(29) Nolas, G.S., G.A. Slack, D.T. Morelli, T.M. Tritt, A.C. Ehrlich, "The effect of rare-earth filling on the lattice thermal conductivity of skutterudites", *Journals of Applied Physics*, **1996**, *79*, 4002-4008.

(30) Sales, B.C., "Filled Skutterudites", *Handbook on the Physics and Chemistry of Rare Earths*, **2003**, *33*, 1-34.

(31) Nolas, G.S., M. Kaeser, R.T. Littleton IV, T.M. Tritt, "High figure of merit in partially filled ytterbium skutterudite materials", *Applied Physics Letters*, **2000**, *77*, 1855-1857.

(32) Sales, B.C, D. Mandrus, R.K. Williams, *Science*, **1996**, *272*, 1325-1358.

(33) Nolas, G.S, D.T. Morelli, T.M. Tritt, *Annual Reviews Materials Research*, **1999**, *29*, 89-106.

(34) Dresselhaus, M., G. Chen, M.Y. Tang, R.G. Yang, H.Y. Lee, D.Z. Wang, "New Directions for Low-Dimentional Thermoelectric Materials", *Advanced Materials*, **2007**, *19*, 1043-1053.

(35) Zheng, J.C., "Recent advances on thermoelectric materials", *Front Phys. China*, **2008**, *3*, 269-279.

(36) Tan G., S. Wang, Y. Yan, H. Li, X. Tang, "Enhanced thermoelectric performance in p-type $Ca_{0.5}Ce_{0.5}Fe_{4-x}Ni_xSb_{12}$ skutterudites by adjusting the carrier concentration", *J. Alloys Compd.*, **2012**, *513*, 328-333.

(37) Anno, H., H. Yamada, T. Nakabayashi, M. Hokazono, R. Shirataki, "Gallium composition dependence of crystallographic and thermoelectric properties in polycrystalline type-1 $Ba_8Ga_xSi_{46-x}$ (nominal x=14-18) clathrates prepared by combining arc melting and spark plasma sintering methods", *J Solid State Chem.*, **2012**, *193*, 94-104.

(38) Wang, S., F. Fu, X. She, G. Zheng, H. Li, X. Tang, "Optimizing thermoelectric performance of Cd-doped β-Zn_4Sb_3 through self-adjusting carrier concentration", *Intermetallics*, **2011**, *19*, 1823-1830.

(39) Caillat T., A. Borshchevsky, J.P. Fleurial, "Proceedings of the Eleventh International Conference on Thermoeletrics", *Arlington Texas*, K.R. Bao ed., **1993**,

(40) D. Jung, M.H. Whangbo, S. Alvarez, *Inorg. Chem.*, **1990**, *29*, 2252-2255.

(41) Shi, X., W. Zhang, L.D. Chen, J. Yang, "Filling fraction limit for intricsic voids in crystals: doping in skutterudites", *Phys. Rev. Lett.*, **2005**, *95*. 185503(4).

(42) Zhang, W., X. Shi Z.G. Mei, Y. Xu, L.D. Chen, J. Yang, G.P. Meisner, *Applied Physics Letters*, **2006**, *89*, 112105.

(43) Pei, Y.Z., L.D. Chen, W. Zhang, X. Shi, S.Q. Bai, X.Y. Zhao, Z.G. Mei, X.Y. Li, *Applied Physics Letters*, **2006**, *89*, 221107.

(44) Sangster, J., A.D. Pelton, "The K-Sb (Potassium-Antimony) system", *Journal of Phase Equilibria*, **1993**, *14(4)*, 510-514.

(45) Parker, W.J., R.J. Jenkins, C.P. Butler, G.L. Abbott, "Flash method of determining thermal diffusivity, heat capacity, and thermal conductivity", *Journal of Applied Physics*, **1961**, *32(9)*, 1679-1684.

(46) Van der Pauw, L.J., "A method of measuring specific resistivity and Hall effect of discs of arbitrary shape", *Philips Res. Repts.*, **1958**, *13*, 1-9.

(47) Wood, C. D. Zoltan, G. Stapfer, "Measurement of Seebeck coefficient using a light pulse", *Rev. Sci. Instrum.*, **1985**, *56*, 719.

Part II. The effects of filling fractions on lattice parameters of n-type filled $IrSb_3$ skutterudites.

Chapter 5. Introduction

Due to the presence of "voids" in the skutterudite structure, foreign atoms can easily fill in and significantly reduce thermal conductivities, while having little impact on electrical conductivities. [1,2,3] As mentioned in Part I, the carrier concentration is the most important factor that is of concern because it can dominate the electronic transport behavior of the TE material by exerting a significant effect on both the electrical conductivity and the Seebeck coefficient;[4] the electrical resistivity, the Seebeck coefficient and the thermal conductivity are mutually related and vary systematically as a function of carrier concentration.[5] It was also found that all TE properties depend closely on the carrier concentration and the optimal carrier concentration for typical TE materials was found to be in the range from 10^{19} to 10^{21} per cm^3.[6] In addition, the carrier concentration can be easily monitored by the level of doping or the filling fraction of the fillers, which can be initially estimated from the lattice parameter data calculated from X-ray diffraction, and the materials' elemental composition obtained from scanning electron microscopy (SEM) and electron microprobe analysis (EPMA), respectively.

Several efforts studying the filling fraction limit of $CoSb_3$ have been carried out and showed strong agreements between the lattice parameter and the filling fraction.[7,8,9] According to Chen *et al.*[10], a filling fraction up to 44% was achieved for barium-filled $CoSb_3$-based skutterudite synthesized using elemental barium as the barium source. They also found that the lattice parameter increases linearly with Ba content. No confirmative result on the filling fraction of europium-filled skutterudite has yet been published. There have been attempts on filling $IrSb_3$-

based skutterudites with various metal fillers, but little work has been done to elucidate the relationship between the lattice parameter and the filling fraction in $IrSb_3$ skutterudites. The experiments repeated here explore how filling fractions affect lattice parameters on barium-filled and europium-filled n-type filled $IrSb_3$ skutterudites. Due to similarities between $CoSb_3$ and $IrSb_3$ skutterudite structures, a linear correlation between the filling fraction and the lattice parameter is expected.

Chapter 6. Experimental

Unfilled $IrSb_3$ skutterudite was prepared by sealing stoichiometric amounts of elemental iridium (99.99%, powder) and antimony (99.999%, shot) in an evacuated quartz tube, and the tube was heated in a furnace at 900^0C for 48 hours.

Barium filled $IrSb_3$ skutterudite samples ($Ba_yIr_4Sb_{12}$, y = 0.15, 0.20, 0.25, 0.30, 0.35, 0.40) were prepared by planetary ball milling stoichiometric amounts of elemental barium (99+%, rod), iridium (99.99%, powder) and antimony (99.999%, shot). The resulting powders were than sealed in evacuated quartz tubes and heated to 900^0C for 48 hours. After furnace treatment, the powders were then hot-pressed according to the hot-pressed profile in Table 4 to produce cylindrical samples. These samples were then analyzed by X-ray diffraction (XRD) for lattice parameters and by scanning electron microscopy (SEM) and electron microprobe analysis (EPMA) for elemental compositions.

Similarly, europium filled $IrSb_3$ skutterudite samples ($Eu_yIr_4Sb_{12}$, y = 0.15, 0.25, 0.30, 0.35) were prepared by planetary ball milling stoichiometric amounts of elemental barium (99+%, rod), iridium (99.99%, powder) and antimony (99.999%, shot). The resulting powders were than sealed in evacuated quartz tubes and heated to 900^0C for 48 hours. After furnace treatment, the powders were then hot-pressed at 880^0C under 1.25 metric tons for 80 minutes to produce cylindrical samples. These samples were then analyzed by X-ray diffraction (XRD) for lattice parameters and by electron microprobe analysis (EPMA) for elemental compositions.

Chapter 7. Results and Discussion

Figures 18 present the relationship between the nominal filling fractions and the EPMA-measured filling fractions in $Ba_yIr_4Sb_{12}$ and $Eu_yIr_4Sb_{12}$ samples. As the nominal filling fraction increases, the EPMA-measured filling fraction also increases. However, among barium-filled samples, the EPMA filling fraction only increased slightly or stayed the same when the nominal one exceeded 0.30. This suggests that the filling fraction limit for the barium filler is somewhere between 0.30 and 0.35 for $IrSb_3$-based skutterudites. This phenomenon did not occur in europium-filled samples as the EPMA filling fraction kept increasing when the nominal filling fraction increased among the samples studied. The barium atom is significantly larger than the europium atom, i.e. the covalent radius of barium is 215 pm, as compared to 198 pm for europium. As a result, more of the smaller europium atoms can fill in the $IrSb_3$ skutterudite structure. However, barium possesses a higher filling efficiency compared to europium; at the same nominal filling fractions, the EPMA filling fractions of barium filled samples were higher than the europium filled samples.

Figures 19 shows the lattice parameter as a function of filling fraction (nominal and EPMA) in $Ba_yIr_4Sb_{12}$ samples. Most of the samples revealed an approximate linear correlation between the lattice parameter and the filling fraction, except for the $Ba_{0.4}Ir_4Sb_{12}$ sample. As explained earlier, as barium exceeded its filling fraction limit, it could no longer incorporate into the structure which in turn negatively affected the filling efficiency and the lattice parameter.

Figure 20 shows the dependence of lattice parameters on the filling fractions among $Eu_yIr_4Sb_{12}$ samples. Initially, the lattice parameter increased significantly when the filling fractions increased. When the nominal filling fraction exceeded 0.30 and the EPMA filling

fraction exceeded around 0.20, the lattice parameters stayed unchanged even though there was a significant difference between the nominal filling fraction and the EPMA filling fraction.

Table 4. Filling Fractions, Lattice Parameters and Hot-Pressed Profiles of $Ba_yIr_4Sb_{12}$ Samples

Nominal Filling Fraction	**EPMA Filling Fraction**	**Lattice parameter (Å)**	**Hot-pressed profile**		
			Temperature (^{0}C)	**Time (min)**	**Force (tons)**
0.15	0.144	9.2617	880	40	1.00
0.20	0.187	9.2664	880	40	1.00
0.25	0.189	9.2646	880	80	1.25
0.30	0.281	9.2713	880	40	1.25
0.35	0.293	9.2751	880	40	1.25
0.40	0.292	9.2664	880	40	1.25

Table 5. Filling Fractions, Lattice Parameters and Hot-Pressed Profiles of $Eu_yIr_4Sb_{12}$ Samples

Nominal Filling Fraction	**EPMA Filling Fraction**	**Lattice parameter (Å)**	**Hot-pressed profile**		
			Temperature (^{0}C)	**Time (min)**	**Force (tons)**
0.15	0.136	9.2565	880	90	1.25
0.25	0.135	9.2616	880	90	1.25
0.30	0.195	9.2628	880	90	1.25
0.35	0.253	9.2627	880	90	1.25

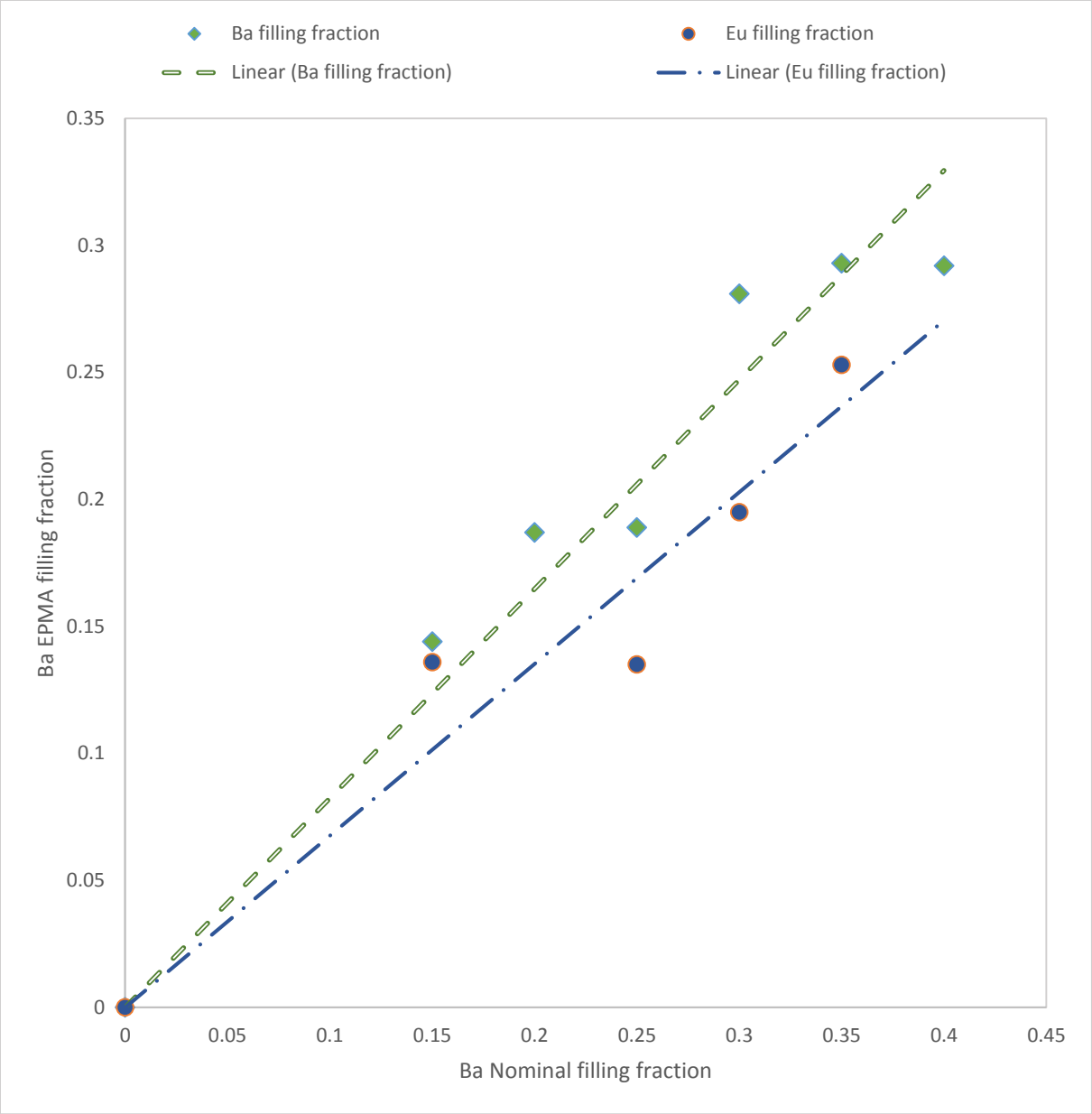

Figures 18. The relationship between the nominal filling fractions and the EPMA-measured filling fractions in $Ba_yIr_4Sb_{12}$ samples.

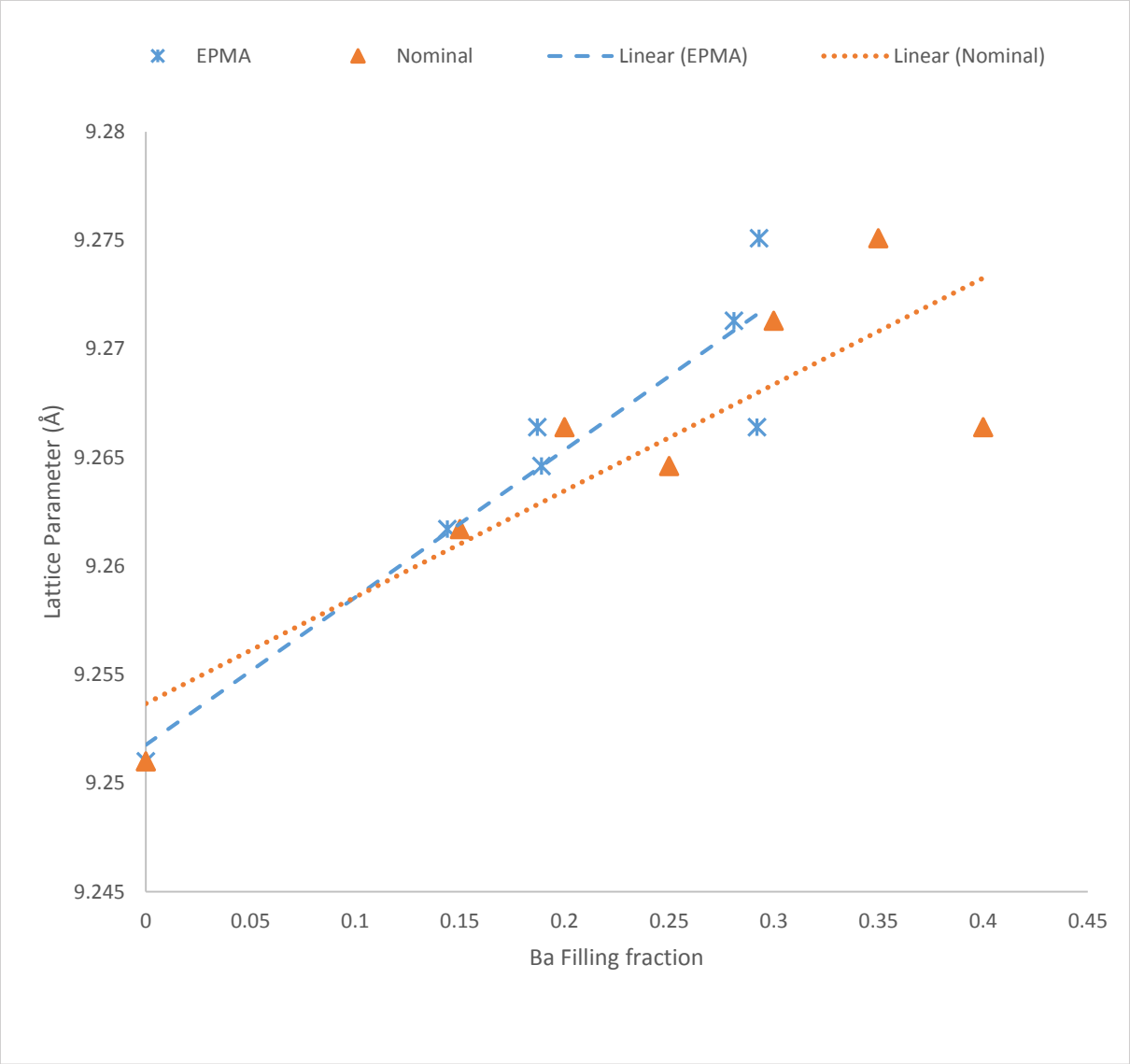

Figures 19. The lattice parameter as a function of filling fraction in $Ba_yIr_4Sb_{12}$ samples (y = 0 – 0.4).

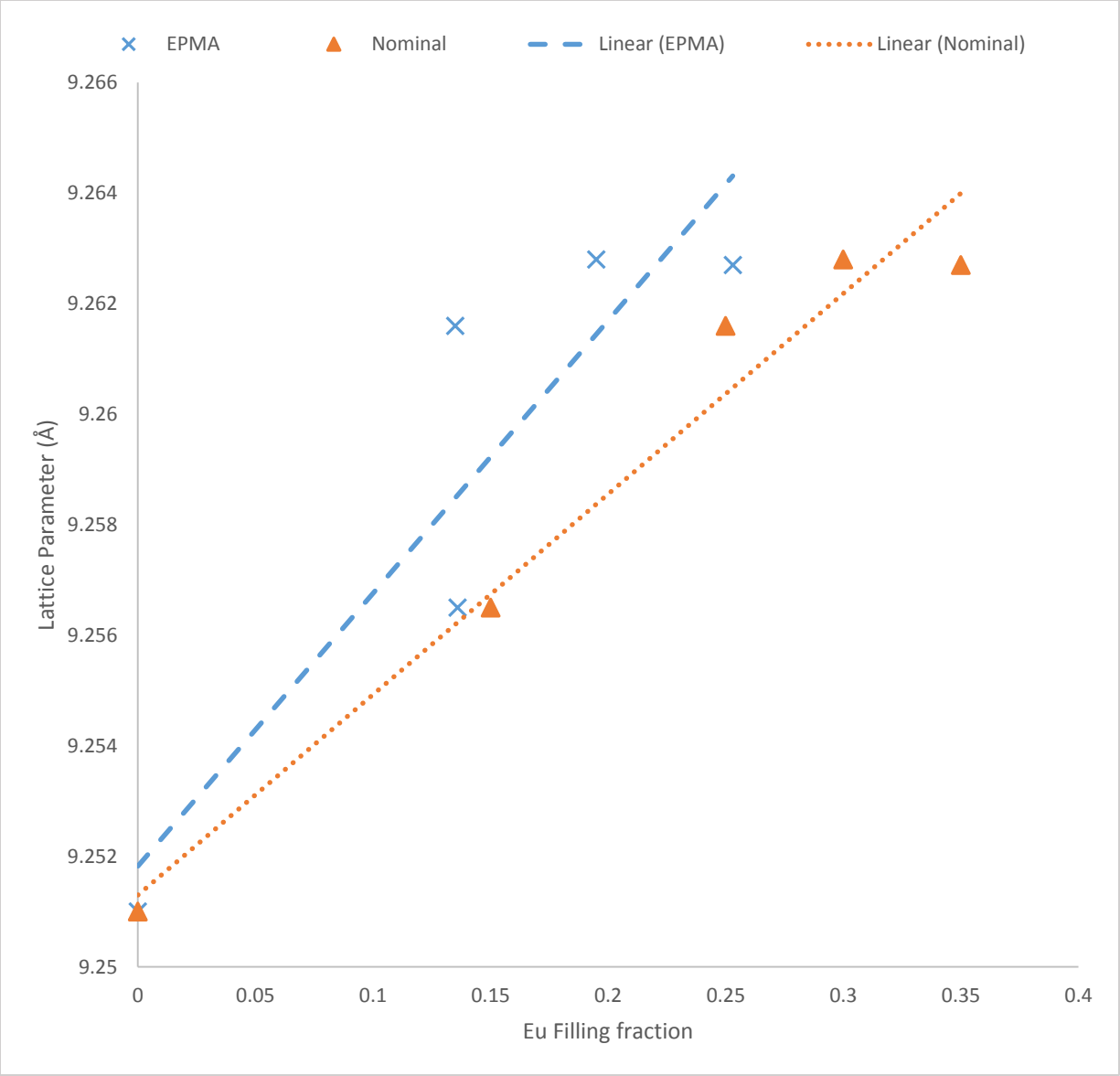

Figures 20. The lattice parameter as a function of filling fraction in $Eu_yIr_4Sb_{12}$ samples.

Chapter 8. Conclusions

Barium-filled and europium-filled skutterudites were synthesized using elemental barium and elemental europium. The final products were analyzed by XRD for lattice parameters and by SEM and EPMA for elemental compositions. As the nominal filling fraction increased, the EPMA filling fraction also increased until the filling fraction limit was reached. The lattice parameters correlate well with the filling fractions for both barium-filled and europium-filled $IrSb_3$ skutterudite samples. Barium experienced higher filling efficiency as compared to europium; however, europium possessed a higher filling fraction limit due to its smaller atomic size. This work demonstrates a close relationship between the lattice parameters and the filling fractions of n-type filled $IrSb_3$ skutterudites.

Part II: References

(1) Uher, C., "Recent Trends in Thermoelectric Material Search I", *Semiconductors and Semimetals*, T.T. Tritt. Ed., **2001**, *69*.

(2) Berardan, D. *et al.*, *Journals of Applied Physics*, **2005**, *98*, 033710.

(3) Slack, G.A., *CRC Handbook of Thermoelectrics*, D.M. Rowe ed., *CRC Press*, **1995**, Chap. 34, 407.

(4) Tan G., S. Wang, Y. Yan, H. Li, X. Tang, "Enhanced thermoelectric performance in p-type $Ca_{0.5}Ce_{0.5}Fe_{4-x}Ni_xSb_{12}$ skutterudites by adjusting the carrier concentration", *J. Alloys Compd.*, **2012**, *513*, 328-333.

(5) Anno, H., H. Yamada, T. Nakabayashi, M. Hokazono, R. Shirataki, "Gallium composition dependence of crystallographic and thermoelectric properties in polycrystalline type-1 $Ba_8Ga_xSi_{46-x}$ (nominal x=14-18) clathrates prepared by combining arc melting and spark plasma sintering methods", *J Solid State Chem.*, **2012**, *193*, 94-104.

(6) Wang, S., F. Fu, X. She, G. Zheng, H. Li, X. Tang, "Optimizing thermoelectric performance of Cd-doped β-Zn_4Sb_3 through self-adjusting carrier concentration", *Intermetallics*, **2011**, *19*, 1823-1830.

(7) Puyet, M., B. Lenoir, A. Dauscher, M. Dehmas, C. Stiewe, E. Muller, *J. Appl. Phys.*, **2004**, *95*, 4852-4855.

(8) Nolas, G.S., M. Kaeser, R.T. Littleton IV, T.M. Tritt, "High figure of merit in partially filled ytterbium skutterudite materials", *Applied Physics Letters*, **2000**, *77*, 1855-1857.

(9) Morelli, D.T., G.P. Meisner, D. Chen, S. Hu, C. Uher, *Phys. Rev. B.*, **1997**, *56*, 7376 - 7383.

(10) Chen, L.D., T. Kawahara, X.F. Tang, T. Goto, *J. Appl. Phys.*, **2001**, *90(4)*, 1864-1868.